

RESEARCH ARTICLE

Exposure to *Mycobacterium* remodels alveolar macrophages and the early innate response to *Mycobacterium tuberculosis* infection

Dat Mai¹, Ana Jahn¹, Tara Murray¹, Michael Morikubo¹, Pamela N. Lim^{2,3}, Maritza M. Cervantes², Linh K. Pham^{2,4}, Johannes Nemeth^{1*}, Kevin Urdahl¹, Alan H. Diercks¹, Alan Aderem¹, Alissa C. Rothchild^{1,2*}

1 Center for Global Infectious Disease Research, Seattle Children's Research Institute, Seattle, Washington, United States of America, **2** Department of Veterinary and Animal Sciences, University of Massachusetts Amherst, Amherst, Massachusetts, United States of America, **3** Molecular and Cellular Biology Graduate Program, University of Massachusetts Amherst, Amherst, Massachusetts, United States of America, **4** Animal Biotechnology and Biomedical Sciences Graduate Program, University of Massachusetts Amherst, Amherst, Massachusetts, United States of America

* Current address: University Hospital Zurich, University of Zurich, Division of Infectious Diseases and Hospital Epidemiology, Zürich, Switzerland
* arothchild@umass.edu



OPEN ACCESS

Citation: Mai D, Jahn A, Murray T, Morikubo M, Lim PN, Cervantes MM, et al. (2024) Exposure to *Mycobacterium* remodels alveolar macrophages and the early innate response to *Mycobacterium tuberculosis* infection. *PLoS Pathog* 20(1): e1011871. <https://doi.org/10.1371/journal.ppat.1011871>

Editor: Padmini Salgame, New Jersey Medical School, UNITED STATES

Received: August 3, 2023

Accepted: November 27, 2023

Published: January 18, 2024

Copyright: © 2024 Mai et al. This is an open access article distributed under the terms of the [Creative Commons Attribution License](https://creativecommons.org/licenses/by/4.0/), which permits unrestricted use, distribution, and reproduction in any medium, provided the original author and source are credited.

Data Availability Statement: Raw and processed RNA-sequencing data can be accessed from the National Center for Biotechnology Information (NCBI) Gene Expression Omnibus (GEO) database under accession number GSE212205.

Funding: This work was supported by National Institute of Allergy and Infectious Disease of the National Institute of Health under Awards U19AI135976 (A.A.), R01AI032972 (A.A.), 75N93019C00070 (K.U., A.C.R., A.A.), and

Abstract

Alveolar macrophages (AMs) play a critical role during *Mycobacterium tuberculosis* (Mtb) infection as the first cells in the lung to encounter bacteria. We previously showed that AMs initially respond to Mtb *in vivo* by mounting a cell-protective, rather than pro-inflammatory response. However, the plasticity of the initial AM response was unknown. Here, we characterize how previous exposure to *Mycobacterium*, either through subcutaneous vaccination with *Mycobacterium bovis* (scBCG) or through a contained Mtb infection (coMtb) that mimics aspects of concomitant immunity, impacts the initial response by AMs. We find that both scBCG and coMtb accelerate early innate cell activation and recruitment and generate a stronger pro-inflammatory response to Mtb *in vivo* by AMs. Within the lung environment, AMs from scBCG vaccinated mice mount a robust interferon-associated response, while AMs from coMtb mice produce a broader inflammatory response that is not dominated by Interferon Stimulated Genes. Using scRNAseq, we identify changes to the frequency and phenotype of airway-resident macrophages following *Mycobacterium* exposure, with enrichment for both interferon-associated and pro-inflammatory populations of AMs. In contrast, minimal changes were found for airway-resident T cells and dendritic cells after exposures. *Ex vivo* stimulation of AMs with Pam3Cys, LPS and Mtb reveal that scBCG and coMtb exposures generate stronger interferon-associated responses to LPS and Mtb that are cell-intrinsic changes. However, AM profiles that were unique to each exposure modality following Mtb infection *in vivo* are dependent on the lung environment and do not emerge following *ex vivo* stimulation. Overall, our studies reveal significant and durable remodeling of AMs following exposure to *Mycobacterium*, with evidence for both AM-intrinsic changes and contributions from the altered lung microenvironments. Comparisons between the scBCG and coMtb models highlight the plasticity of AMs in the airway and opportunities to target their function through vaccination or host-directed therapies.

R21AI163809 (A.C.R.). J.N. was supported by the Swiss National Foundation under grant 310030_200407. P.L. was supported by National Research Service Award T32 GM135096 from the National Institutes of Health. The funders had no role in study design, data collection and analysis, decision to publish, or preparation of the manuscript.

Competing interests: I have read the journal's policy and the authors of this manuscript have the following competing interests: J.N. received honoraria for presentations from Oxford Immunotec, Gilead and Viiv.

Author summary

Tuberculosis, a disease caused by the bacteria *Mycobacterium tuberculosis* (Mtb), claims around 1.6 million lives each year, making it one of the leading causes of death worldwide by an infectious agent. Based on principles of conventional immunological memory, prior exposure to either Mtb or *M. bovis* BCG leads to antigen-specific long-lasting changes to the adaptive immune response that can be effective at protecting against subsequent challenge. However, how these exposures may also impact the innate immune response is less understood. Alveolar macrophages are tissue-resident myeloid cells that play an important role during Mtb infection as innate immune sentinels in the lung and the first host cells to respond to infection. Here, we examined how prior *Mycobacterium* exposure, either through BCG vaccination or a model of contained Mtb infection, impacts the early innate response by alveolar macrophages. We find that prior exposure remodels the alveolar macrophage response to Mtb through both cell-intrinsic changes and signals that depend on the altered lung environment. These findings suggest that the early innate immune response could be targeted through vaccination or host-directed therapy and could complement existing strategies to enhance the host response to Mtb.

Introduction

Mycobacterium tuberculosis (Mtb), the causative agent of Tuberculosis (TB), claimed more than 1.6 million lives in 2021. For the first time since 2005, the number of TB deaths worldwide is increasing [1,2]. These trends highlight the urgent need for new vaccine and therapeutic strategies. Traditionally, vaccine design has focused on generating a rapid, robust, and effective adaptive immune response. However, recent studies suggest that the innate immune system can undergo long-term changes in the form of trained immunity [3], which affect the outcome of infection and could function as important components of an effective TB vaccine [4,5]. Initial trained immunity studies focused on central trained immunity, long-term changes to hematopoietic stem cells that lead to functional changes in short-lived innate cell compartments (i.e., monocytes, NK cells, dendritic cells) [3]. More recent studies have examined innate training in tissue-resident macrophages and demonstrated that these cells are also affected by prior exposures. Tissue-resident macrophages can respond to remote injury and inflammation [6], undergo long-term changes [3], and display altered responses to bacteria after pulmonary viral infection [7–9].

Lung resident alveolar macrophages (AMs) are the first cells to become infected with inhaled Mtb and engage a cell-protective response, mediated by the transcription factor Nrf2, that impedes their ability to effectively control bacterial growth [10,11]. In this study, we examined how prior mycobacterial exposure reprograms AMs and alters the overall innate response in the lung to aerosol challenge with Mtb. To evaluate the range of AM plasticity, we chose to compare the effects of subcutaneous BCG vaccination (scBCG) with those arising from a contained Mtb-infection (coMtb) model. BCG, a live-attenuated TB vaccine derived from *M. bovis* and typically given during infancy, provides protection against disseminated pediatric disease but has lower efficiency against adult pulmonary disease [12–14]. In addition to enhancement of Mtb-specific adaptive responses, based on shared antigens, BCG vaccination also leads to changes in hematopoiesis and epigenetic reprogramming of myeloid cells in the bone marrow [15], early monocyte recruitment and Mtb dissemination [16], and innate activation of dendritic cells critical for T cell priming [17]. Intranasal BCG vaccination protects

against *Streptococcus pneumoniae* and induces long term activation of AMs [18]. A recent study has shown that one mechanism by which BCG vaccination can elicit innate training effects on AMs, separate from alterations to the monocyte population, is through changes to the gut microbiome and microbial metabolites [19]. BCG vaccination is also associated with trained immunity effects in humans [20–22], including well-described reductions in all-cause neonatal mortality and protection against bladder cancer [3,23].

The coMtb model is generated by intradermal inoculation with virulent Mtb into the ears of mice and leads to a contained but persistent lymph node Mtb infection [24,25]. The model replicates observations in both humans and non-human primates (NHPs) that prior exposure to Mtb infection provides protection against subsequent exposure, through a form of concomitant immunity [26,27]. In a previous study, we found that coMtb leads to protection against challenge with aerosol Mtb infection and protects mice against heterologous challenges, including infection with *Listeria monocytogenes* and expansion of B16 melanoma cells, results which suggest there is substantial remodeling of innate immune responses [25]. We found that AMs from coMtb mice mount a more inflammatory response to Mtb infection compared to AMs from control mice, and the enhancement in AM activation after infection, as measured by MHC II expression, was dependent on IFN γ R signaling [25].

Here, we show that while both coMtb and scBCG protect against low dose Mtb aerosol challenge, they remodel the *in vivo* innate response in different ways. In AMs, scBCG elicits a very strong interferon response in AMs, while coMtb promotes a broader pro-inflammatory response that is less dominated by Interferon Stimulated Genes. Prior exposure to *Mycobacterium* also remodels the frequency and phenotype of AM subsets in the lung prior to aerosol challenge and leads to significant changes in the early dynamics of the overall innate response. While changes in the AM responses that are unique to each exposure (scBCG, coMtb) depend on the lung environment, stronger interferon-associated responses following both LPS and Mtb stimulation *ex vivo* reveal cell-intrinsic changes.

Results

Prior exposure to *Mycobacterium* accelerates activation and innate cell recruitment associated with Mtb control

We first determined the earliest stage of infection when the immune response was altered by prior exposure to *Mycobacterium*. Mice were vaccinated with scBCG or treated with coMtb, rested for 8 weeks, and then challenged with low-dose H37Rv aerosol infection. We measured both the cellularity and activation of innate immune cells in the lung at 10, 12 and 14 days following infection, the earliest timepoints when innate cells are known to be recruited [10,11,28]. We observed a significant increase in MHC II Median Fluorescence Intensity (MFI) as early as day 10 for AMs from coMtb mice and day 12 for AMs from scBCG mice compared to controls (Figs 1A and S1). There were no significant differences in MHC II expression prior to challenge on day 0 (Fig 1A). There were also significant increases in the numbers of monocyte-derived macrophages (MDM), neutrophils (PMN), dendritic cells, and Ly6C⁺ CD11b⁺ monocytes by day 10 in coMtb mice compared to controls, with further increases by days 12 and 14 (Figs 1B and S1). scBCG elicited similar increases in these populations starting at day 10, but the increases were not as robust or rapid as those observed in coMtb. Significant differences between scBCG and coMtb groups were found at days 10, 12, and 14 in MDM, day 14 in PMN, days 12 and 14 in dendritic cells, and day 14 in Ly6C⁺ CD11b⁺ monocytes (Fig 1B). While there were not significant differences in AM cell number between the three conditions, there was a modest drop in viability for both AMs from scBCG and coMtb mice by day 14 (Fig 1C).

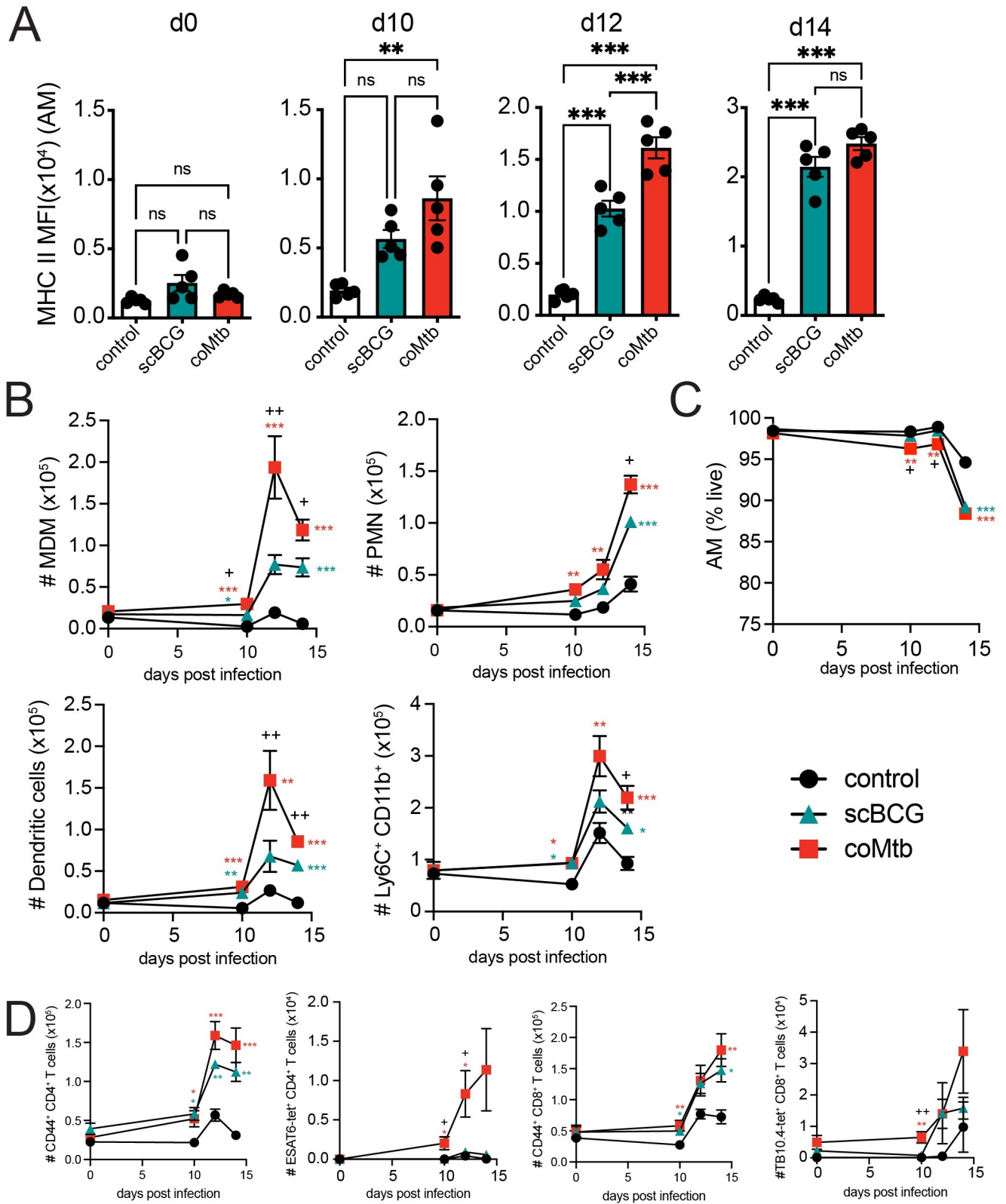


Fig 1. Prior exposure to *Mycobacterium* leads to faster activation and innate cell recruitment following aerosol Mtb challenge. Control, scBCG, and coMtb mice, 8 weeks following exposure, challenged with standard low-dose H37Rv. Lungs collected on day 10, 12, and 14 post-infection. A) AM MHC II MFI. B) Total numbers of MDMs, PMN, DC, and Ly6C⁺CD11b⁺ monocytes. C) AM viability (% Zombie Violet-). D) Total numbers of CD44⁺ CD4⁺ T

cells, ESAT6-tetramer⁺ CD4⁺ T cells, CD44⁺ CD8⁺ T cells, and TB10.4-tetramer⁺ CD8⁺ T cells. Mean +/- SEM, 5 mice per group, representative of 3 independent experiments. One-way ANOVA with Tukey post-test. * p < 0.05, ** p < 0.01, *** p < 0.001. B, C) *, **, and *** scBCG or coMtb vs control; +, + scBCG vs coMtb.

<https://doi.org/10.1371/journal.ppat.1011871.g001>

In addition to early changes in innate cell activation and recruitment, we observed early recruitment of activated CD44⁺ CD4⁺ and CD8⁺ T cells in the lungs of both coMtb and scBCG mice starting at day 10 as well as TB antigen-specific T cells, ESAT6-tetramer⁺ CD4⁺ T cells and TB10.4-tetramer⁺ CD8⁺ T cells in coMtb mice starting at day 10 compared to controls and scBCG mice (Figs 1D and S1). The differences in the recruitment of ESAT6-tetramer⁺ CD4⁺ T cells between scBCG and coMtb were expected, as the ESAT6 antigen is expressed by H37Rv but not by BCG.

We also evaluated whether these cell recruitment differences correlated with changes in bacterial burden. To compile CFU results from three independent experiments, each with slightly different bacterial growth (S2A Fig), we calculated a ΔCFU value that compared the bacterial burden of each sample to the average for the respective control based on timepoint, organ, and experiment. We found that both modalities generated a significant reduction in bacterial burden compared to controls in the lung, spleen, and lung-draining lymph node (LN) at day 14 and at day 28, as previously reported [16,25,29] (S2A–S2D Fig). At day 10, we observed no difference in lung bacterial burden in scBCG or coMtb mice compared to controls and a small increase in coMtb mice over scBCG. The majority of control mice had undetectable bacteria in spleen and LN at this time. There was a significant reduction in bacterial burden in the lung by day 12 in coMtb but not scBCG mice and a significant reduction in CFU in the LN in both models compared to controls (S2B Fig). Our results demonstrate that prior *Mycobacterium* exposure leads to accelerated innate cell activation and recruitment, alongside an increase in activated T cells, within the first two weeks of infection, with coMtb generating a faster and more robust response compared to scBCG. These early immune changes are associated with reductions in bacterial load in the lung. Differences in bacterial burden in the LN and spleen suggest delays in bacterial dissemination, which first appear in the LN at day 12 and then in the spleen at day 14 (S2A Fig).

***Mycobacterium* exposure alters the *in vivo* alveolar macrophage response to Mtb infection**

To examine the earliest response to Mtb, we measured the gene expression profiles of Mtb-infected AMs isolated by bronchoalveolar lavage and cell sorting, as previously described [10], 24 hours following aerosol challenge with high dose mEmerald-H37Rv (depositions: 4667, 4800) in scBCG-vaccinated mice and compared these measurements to previously generated profiles of AMs from control (unexposed) mice [10] and coMtb mice [25] (S1 Table). As previously observed for the high dose infection, an average of 1.79% (range: 0.91–3.18%) of total isolated AMs were Mtb infected 24 hours after infection. Changes induced by Mtb infection were measured by comparing gene expression between Mtb-infected AMs and respective naïve AMs for each of the three groups (control, scBCG, coMtb). Principal Component Analysis on Mtb infection-induced changes showed that each of the three conditions led to distinct expression changes (Fig 2A) and the majority of up-regulated Differentially Expressed Genes (DEG) (fold change > 2, FDR < 0.05) were unique to each condition (control: 151 unique/257 total DEG, scBCG: 222/289, coMtb: 156/229) (Fig 2B). The divergence in the responses of Mtb-infected AMs from each of the 3 conditions was also reflected in the diversity in the Top 20 Canonical Pathways identified by Ingenuity Pathway Analysis (S3 Fig).

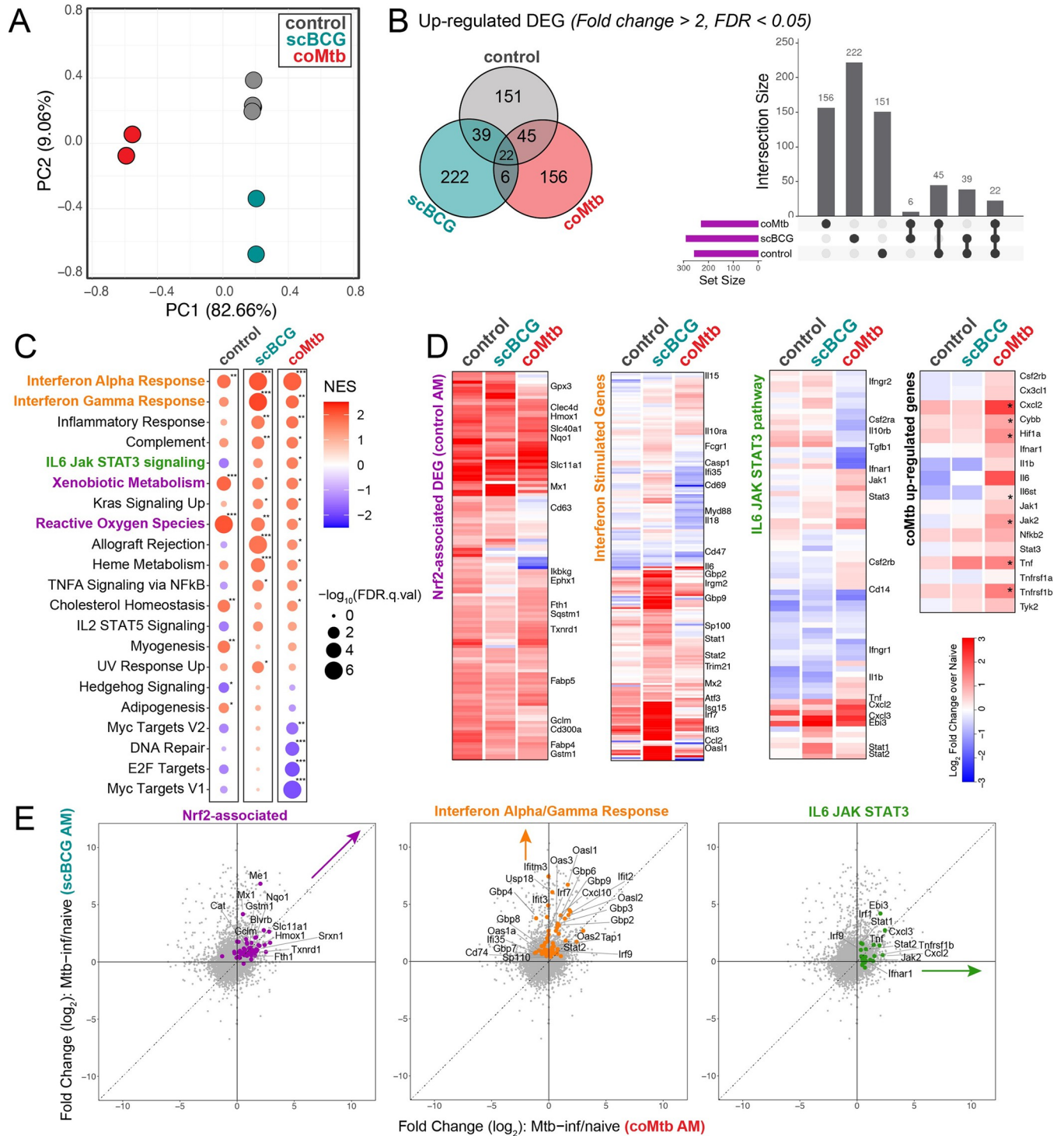


Fig 2. *Mycobacterium* exposure alters the alveolar macrophage transcriptional response to Mtb infection *in vivo*. Bulk RNA-seq profiles of Mtb-infected AMs 24 hours following high-dose mEmerald-H37Rv infection. Gene expression changes are compared to respective naïve samples: Mtb-inf control vs naïve control; Mtb-inf scBCG vs naïve scBCG; Mtb-inf coMtb vs naïve coMtb (controls- reported in Rothchild et al, 2019 [10]; coMtb- reported in Nemeth et al, 2020 [25]). A) Principal Component Analysis using DEG (|fold change| > 2, FDR < 0.05) in Mtb-infected AMs compared to respective naïve AMs (control, scBCG, or coMtb). B) Venn Diagram and Intersection plot of overlap in up-regulated DEG between the 3 conditions. C) Gene Set Enrichment Analysis of 50 Hallmark Pathways. Pathways shown have |NES| > 1.5 and FDR < 0.05 for at least one of the conditions. * FDR < 0.05, ** FDR < 0.01, *** FDR < 0.001. D) Heatmap of 131 original *in vivo* DEG at 24 hours in Mtb-infected AM (left), Interferon Stimulated Genes, derived from macrophage response to IFN α (fold change > 2, p-value < 0.01) Mostafavi et al, 2016 [30] (center-left), IL6 JAK STAT3 hallmark pathway (center-right) and selected coMtb signature genes (right, *FDR < 0.05,

FC > 2). E) Scatterplots depicting fold change (\log_2) for Mtb-infected AMs over naïve AMs for scBCG versus coMtb. Highlighted pathways: Nrf2-associated genes out of 131 original *in vivo* DEG (56 genes, purple), shared leading edge genes for scBCG Interferon Alpha Response and Interferon Gamma Response pathways (61 genes, orange), and leading edge genes for coMtb IL6 JAK STAT3 pathway (23 genes, green). Compiled from 4 independent experiments per condition for control, 2 independent experiments per condition for scBCG and coMtb.

<https://doi.org/10.1371/journal.ppat.1011871.g002>

To identify trends between groups, we performed Gene Set Enrichment Analysis using a set of 50 Hallmark Pathways. As we've shown previously, Mtb-infected AMs from control mice at 24 hours had strong enrichment for "Xenobiotic Metabolism" and "Reactive Oxygen Species" pathways, indicative of the Nrf2-associated cell-protective response (Fig 2C). While these two pathways were not among the most enriched pathways in the exposed groups, Mtb-infected AMs from all groups upregulated genes associated with the 131 *in vivo* DEG that make up the cell-protective Nrf2-driven response at 24 hours [10] (Fig 2D). Expression profiles for Mtb-infected AMs from scBCG mice showed the strongest enrichment for "Interferon Alpha Response" and "Interferon Gamma Response" pathways, which contain many shared genes (Fig 2C). The strength of the interferon response was further highlighted by examining gene expression changes in a set of Interferon Stimulated Genes (ISGs) identified from macrophages responding to IFN α (fold change > 2, p-value < 0.01) [30] (Fig 2D). Expression profiles for Mtb-infected AMs from coMtb mice showed a weaker enrichment for interferon response pathways with fewer up-regulated ISGs compared to scBCG, and instead showed enrichment across a number of inflammatory pathways including "IL6 JAK STAT3 signaling" in comparison to the other groups (Fig 2C and 2D). A direct comparison between the gene expression patterns for AMs from scBCG versus coMtb mice could be visualized more readily by scatterplots highlighting either Nrf2-associated, Interferon Alpha and Gamma Response, or IL-6 JAK STAT3 pathway genes (Fig 2E).

In summary, *Mycobacterium* exposures alter the initial *in vivo* response of AMs to Mtb infection 24 hours after challenge and remodel the AM response in distinct ways. AMs from scBCG vaccinated animals mount a strong interferon-associated response, while AMs from coMtb mice express a more diverse inflammatory profile consisting of both interferon-associated genes as well as other pro-inflammatory genes, including those within the IL-6 JAK STAT3 pathway.

***Mycobacterium* exposure modifies the baseline phenotype of alveolar macrophages in the airway**

Although scBCG and coMtb exposures alter the AM responses to Mtb infection *in vivo*, transcriptional effects are not widely evident prior to infection as measured by bulk RNA-sequencing of naïve AMs from control, scBCG, or coMtb mice, including expression of innate receptors and adaptors (S4 Fig). However, we posited that remodeling effects were likely not homogenous across the entire AM population and that small heterogenous changes to baseline profiles might be detectable using a single cell approach. We therefore analyzed pooled BAL samples taken from 10 age- and sex-matched mice from each of the three conditions (control, scBCG, coMtb) eight weeks following *Mycobacterium* exposure by single cell RNA-sequencing (scRNAseq). Gross cellularity was unaffected by mycobacterial exposure as measured by flow cytometry analysis of common lineage markers with AMs being the dominant hematopoietic cell type (57.4–85.8% of CD45⁺ live cells), followed by lymphocytes (5.26–22.7% of CD45⁺ live cells) with smaller contributions from other innate cell populations (S5 Fig).

Six samples, with an average of 2,709 cells per sample (range: 2,117–4,232), were analyzed together for a total of 17,788 genes detected. The most prominent expression cluster mapped to an AM profile, with smaller clusters mapping to T and B lymphocytes, dendritic cells, and

neutrophils (Fig 3A). All cells that mapped to a macrophage profile were extracted and reclustered into 11 macrophage subclusters (Fig 3B and 3C). All but two of the macrophage subclusters (clusters 6 and 8) expressed AM lineage markers (*Siglecf*, *Mertk*, *Fcgr1* (CD64), *Lyz2* (LysM), and *Itgax* (CD11c) and had low expression of *Itgam* (CD11b) (Fig 3D). Cluster 6 showed high *Itgam* and *Lyz2* expression and lower *Siglecf* expression, likely representing a small monocyte-derived macrophage population in the airway, while cluster 8 displayed high *Lyz2* expression, low expression for other AM markers, and expression of *Sftpa1* and *Wfdc2* (S2 Table), genes most commonly expressed by pulmonary epithelial cells, suggesting that this cluster represents a small population of epithelial cells.

To interpret the various expression subclusters, we identified the genes that most distinguished each cluster from the others (S6 Fig and S2 Table). As has been reported by other groups [31,32], a small proportion of the AMs in two clusters (Clusters 4, 9) had high expression of cell cycle genes (i.e., *Top2a*, *Mki67*), indicative of cell proliferation (Fig 3E and S2 Table). Cluster 0 was the most abundant macrophage cluster with high expression of lipid metabolism genes (i.e., *Abcg1*, *Fabp1*) (Fig 3F and S2 Table). Cluster 2 was significantly increased in relative frequency for scBCG samples compared to coMtb ($p = 0.032$, *One-way ANOVA with Tukey post-test*) and associated with oxidative stress response genes (*Hmox1*, *Gclm*). Several Cluster 2 associated genes, *Slc7a11*, *Hmox1*, and *Sqstm1* also had higher overall expression level in scBCG samples compared to either control or coMtb (Fig 3G and S2 Table). Cluster 7 was the only cluster with an increase in relative frequency trending for both scBCG and coMtb ($p = 0.076$, *One-way ANOVA*). Cells in this cluster had high expression of Interferon Stimulated Genes (*Ifit1*, *Isg15*) and within this cluster, cells from scBCG samples had higher expression of *Axl* and *Ifi204* than cells from coMtb samples. (Fig 3H and S2 Table). Cluster 3 had significantly higher relative frequency for coMtb samples compared to control and scBCG samples ($p = 0.021$, 0.039 , respectively, *One-way ANOVA with Tukey post-test*) and was distinguished by expression of macrophage-associated transcription factors (*Cebpb*, *Zeb2*, *Bhlhe40*) [33,34], mitochondrial oxidative phosphorylation (*mt-Co1*, *mt-Cyb*, *mt-Nd2*), chromatin remodeling (*Ankrd11*, *Baz1a*), and immune signaling including the CARD9 complex (*Malt1*, *Bcl10*, *Prkcd*) (Figs 3I and S7 and S2 Table). This expression profile closely matches a subcluster of AMs previously described by Pisu et al, as an “interstitial macrophage-like” AM population (labeled “AM_2”) that expanded in relative frequency in lung samples 3 weeks following low-dose H37Rv infection [31]. Relative expression level for *Cebpb*, *Mt-Cyb*, and *Lars2* within Cluster 3 was higher for cells from coMtb samples compared to either control or scBCG samples.

Interestingly, Cluster 2 (higher relative frequency in scBCG) and Cluster 3 (higher relative frequency in coMtb) represent divergent endpoints of a pseudotime plot generated by a trajectory inference analysis, regardless of whether the starting point is the most abundant cluster in the control group (Cluster 0) (Fig 3J, top) or the cluster of proliferating cells (Cluster 4) (Fig 3J, bottom). This result suggests that scBCG and coMtb may drive AM phenotypes in divergent directions and indicates that AM responses can be remodeled into more than one flavor, rather than only a binary “on/off” state.

To further investigate whether a sub-cluster of AMs might be responsible for the increased enrichment for Interferon Alpha/Gamma Response pathways in the *in vivo* Mtb response in scBCG and coMtb mice, we scored each cluster based on the ISG gene module, previously used in Fig 2D. As expected, we observed that only Cluster 7 showed strong enrichment for ISGs, which trended up in frequency for both scBCG and coMtb samples (Fig 3K).

To investigate potential reprogramming of non-AM macrophages, we examined Cluster 6, the macrophage cluster with low *Siglecf* and high *Itgam* expression that is consistent with a monocyte-derived macrophage population. We observed no statistically significant differences

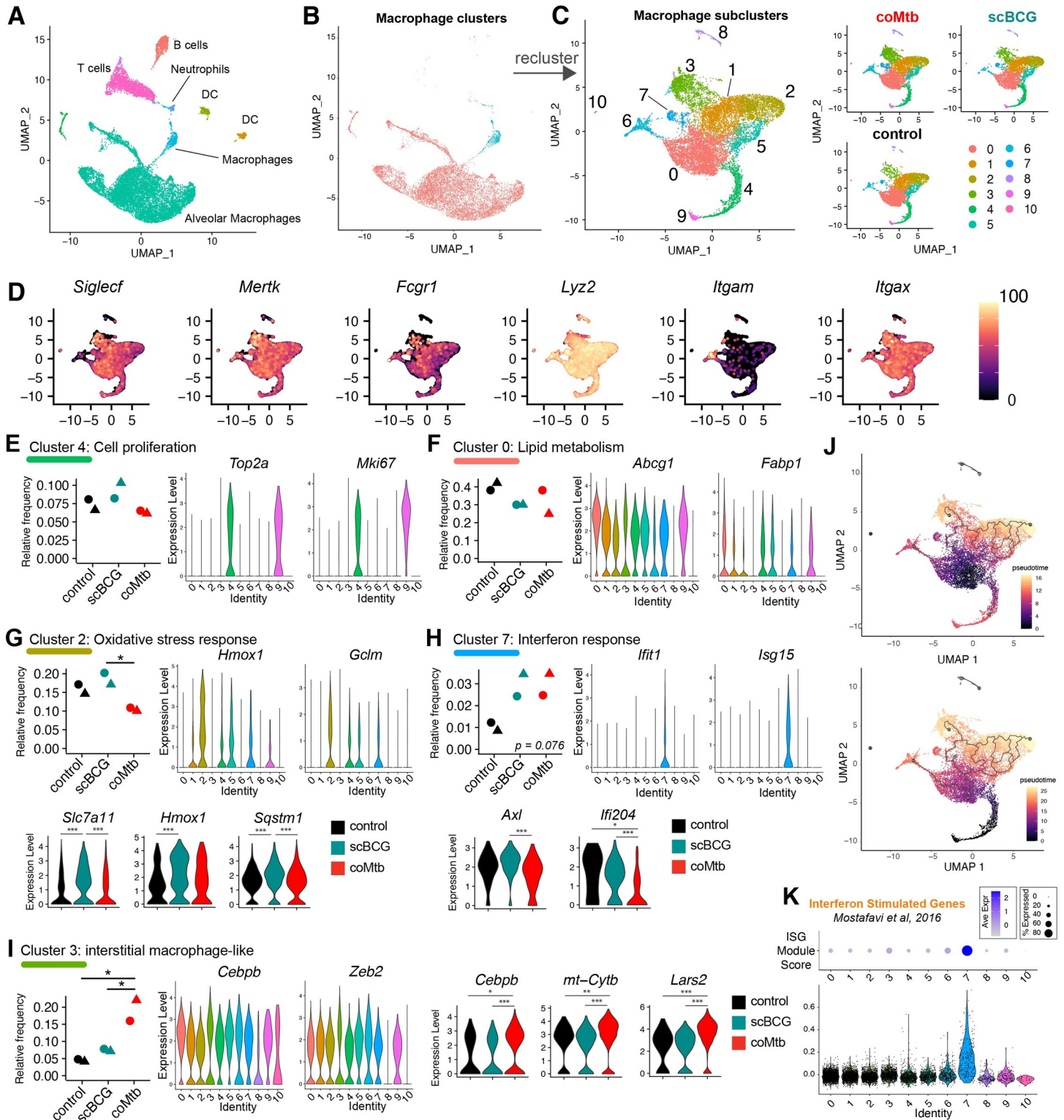


Fig 3. *Mycobacterium* exposure modifies the alveolar macrophage phenotype in the airway pre-challenge. Single-cell RNA-sequencing of BAL samples from control, scBCG, and coMtb mice pre-aerosol challenge. A) Compiled scRNAseq data for all BAL samples, highlighted by major clusters, annotated based on closest Immgen sample match. B) Highlighting of the two clusters used for macrophage subcluster analysis. C) The 11 clusters generated by the macrophage subcluster analysis, separated by condition. D) Expression of major macrophage-specific markers: *Siglecf*, *Mertk*, *Fcgr1*, *Lyz2*, *Itgam* (CD11b), and *Itgax* (CD11c). E-I) Relative frequency of each macrophage subcluster by condition. (*violin plots by cluster*) Expression level of representative genes distinguished by that cluster compared to other clusters. One-way

ANOVA with Tukey post-test, * $p < 0.05$. (3-way violin plots by condition) Differentially expressed genes within Clusters 2, 7, and 3 between control vs scBCG vs coMtb samples. Wilcoxon Rank Sum Test, Bonferroni adjusted p-value. *adj-p < 0.05, **adj-p < 0.01, ***adj-p < 0.001. J) Pseudotime analysis (Monocle3) with starting node at the largest cluster in control, Cluster 0 (top) and at the cluster of proliferating cells, Cluster 4,9 (bottom). K) ISG Module Score by cluster. Module derived from macrophage response to IFN α (fold change > 2, p-value < 0.01) (Mostafavi et al, 2016) [30]. Data is compiled from two independent experiments (circle, triangle) with 3 conditions each for a total of 6 samples.

<https://doi.org/10.1371/journal.ppat.1011871.g003>

in the relative size of this cluster between each of the three conditions (S8A Fig). However, there were a number of Differentially Expressed Genes (DEGs) between the groups, including decreases in expression of CD11b (*Itgam*) and Macrophage scavenger receptor (*Msr1*) for scBCG and coMtb macrophages compared to controls, increases in MHC-related genes (*H2-Aa*, *Cd74*) and iron-metabolism associated genes (*Cd63*, *Fth1*, *Ftl1*) for coMtb macrophages compared to controls (S8B Fig). A previous study found IV BCG induced chromatin accessibility changes in AMs and IMs for some of these genes [31].

Additionally, we compared baseline changes to AMs following scBCG and coMtb exposures to AM changes following ivBCG vaccination (S9 Fig). Overall, we found that ivBCG exposure led to similar changes in AM populations to that of scBCG vaccination, with increased frequency of AMs clustering to “oxidative stress response” and “interferon stimulated genes (ISGs)” (S9C Fig). These baseline changes by scRNAseq mirror what is observed for the response of Mtb-infected AMs from ivBCG mice 24 hours after infection by bulk RNA-seq (S9A and S9B Fig). Profiles of Mtb-infected AMs from ivBCG vaccinated mice most closely match those of Mtb-infected AMs from scBCG vaccinated mice, with robust up-regulation of Interferon Stimulated Genes. These results demonstrate that both SC and IV BCG vaccination lead to similar remodeling of AMs, with profiles distinct from that of coMtb exposure.

In summary, scRNAseq analysis of macrophages isolated by BAL demonstrate that *Mycobacterium* exposure leads to subtle changes in a small minority of AM subsets in the airway, including ones associated with interferon responses and an interstitial macrophage phenotype, while leaving the most abundant subsets of AMs unchanged in frequency or gene expression. We hypothesize that these small changes in baseline profiles may be sufficient to drive the more substantial changes observed in the AM Mtb response *in vivo*, as described in Fig 2.

***Mycobacterium* exposure has minimal impact on T cell populations in the airway**

While AMs are the dominant immune cell type in the airway, other cell populations make up an average of 18.4% of the cells within the BAL in controls (range: 10.4–26.3%) and 31.3% in exposed groups (range: 14.0–48.8%). To examine how *Mycobacterium* exposure influenced other cells in the airway, we focused on T cells and dendritic cells (DCs) which have two of the highest relative frequencies after AMs (Fig 4A and 4B). T cells and DCs were each combined from two original clusters each. Neither population showed a statistically significant difference in relative frequency (Fig 4B). To examine qualitative changes in the T cell population in greater detail, we next reclustered the T cells, resulting in 7 T cell clusters. We manually annotated each of the clusters based on the most closely matched Immgen profiles and the expression of key lineage specific markers (Figs 4A–4C and S10). We focused on the 5 most abundant T cell subclusters (Clusters 0–4). While we observed subtle shifts in the relative frequency of each group, none reached statistical significance. Cluster 0, the most abundant cluster, had an expression profile most consistent with $\gamma\delta$ T cells, including expression of *Cd3e* with low to nil *Cd4* and *Cd8a* and some expression of *Zbtb16* (PLZF) and *Tmem176a*, an ion channel regulated by ROR γ t and reported to be expressed by lung $\gamma\delta$ T cells [35,36] (Figs 4D–

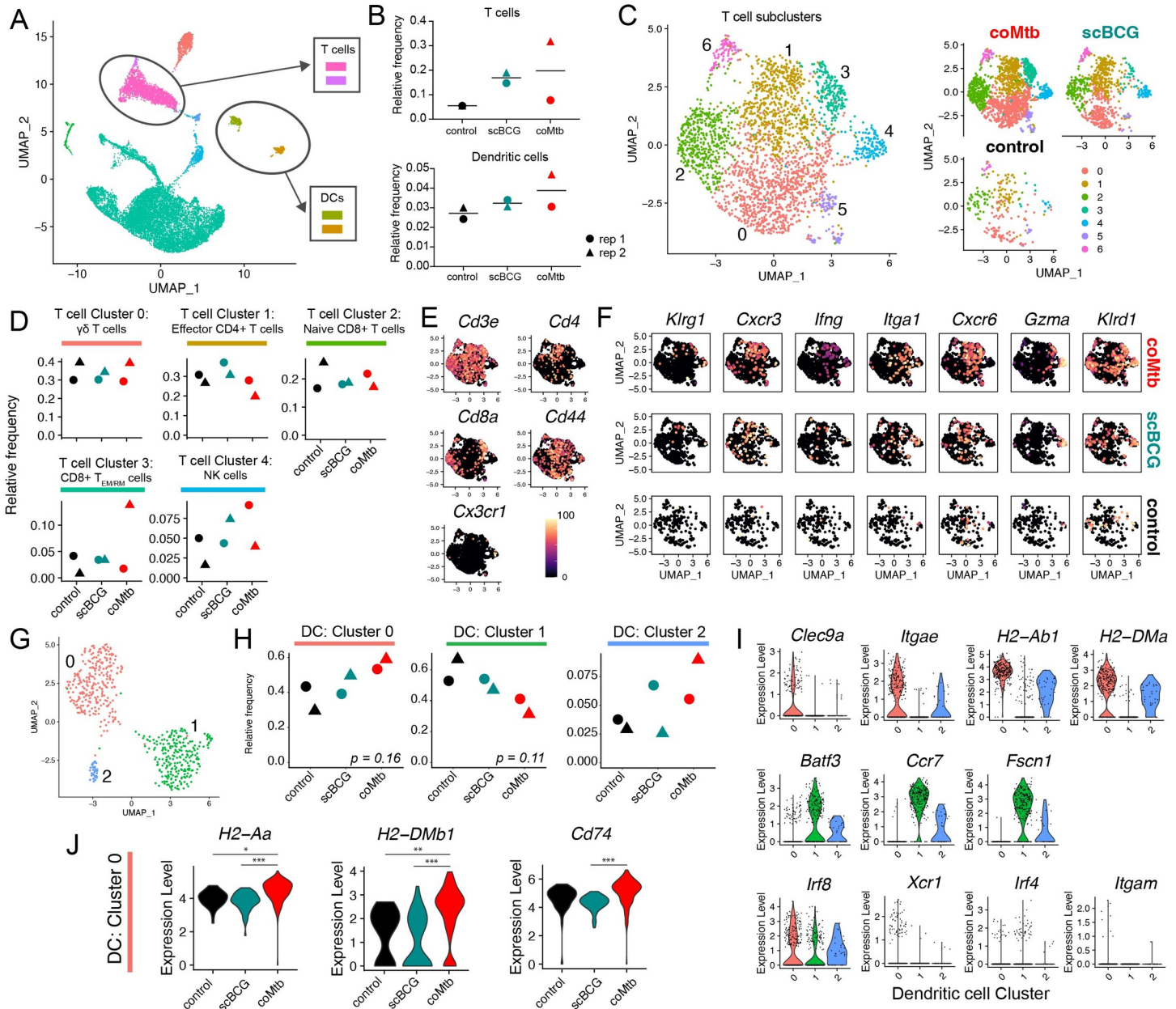


Fig 4. Airway T cell and dendritic cell profiles following *Mycobacterium* exposure. Single-cell RNA-sequencing of BAL samples from control, scBCG, and coMtb mice pre-aerosol challenge. A) Compiled scRNAseq data for all BAL samples, with T cell and dendritic cell clusters highlighted. B) Relative frequency of T cells and DCs. C-F) T cell subcluster analysis. C) T cell subclusters compiled and split by condition. Annotations made following Immgen profile matches and manual marker inspection. D) Relative frequency of Clusters 0–4 for each condition. E) UMAP gene expression plot for general T cell markers. F) UMAP gene expression plot cluster-specific markers split by condition. G–J) Dendritic cell subcluster analysis. G) Dendritic cell subcluster, colored by each of 3 different clusters. H) Relative frequency of Clusters 0–2 for each condition. I) Violin plots for cluster-specific markers and genes of interest. J) Differentially expressed genes in Cluster 0 split by condition. *adj-*p*< 0.05, **adj-*p*< 0.01, ***adj-*p*< 0.001, Wilcoxon Rank Sum Test, Bonferroni adjusted *p*-values. Data is compiled from two independent experiments with 3 conditions each for a total of 6 samples.

<https://doi.org/10.1371/journal.ppat.1011871.g004>

4F and S10). Cluster 1 matched a profile for effector CD4⁺ T cells (Figs 4D–4F and S10), and Cluster 2 matched a profile for naïve CD8⁺ T cells (Figs 4D–4F and S10). Cluster 3 had a profile consistent with effector memory/resident memory CD8⁺ T cells (T_{EM/RM}) (Figs 4D–4F and S10) and Cluster 4 had a profile consistent with NK cells. Overall, there were no

significant changes in the relative frequency of T cell or NK subclusters, despite detection of a number of different lymphocyte subsets in the airway.

***Mycobacterium* exposure modifies the dendritic cell airway landscape**

Re-clustering of DCs yielded 2 major clusters (Cluster 0, 1) and 1 minor cluster (Cluster 2), which had a mixed phenotype with expression of genes from both major clusters (Fig 4G). Cells in Cluster 0 had high expression of *Clec9a*, *Itgae* (CD103), and MHC II genes (*H2-Ab1*, *H2-DMa*) consistent with an expression profile of lung CD103⁺ cDCs [37] (Fig 4I), while cells in Cluster 1 had higher expression of *Batf3*, *Ccr7*, and *Fscn1*. All three of the clusters had high *Irf8* expression and lower expression of *Xcr1*, *Irf4*, and *Itgam* (CD11b) (Fig 4I). While the coMtb samples trended higher in relative frequency for Cluster 0 and low for Cluster 1, compared to the control or scBCG samples, these differences did not meet statistical significance (One-way ANOVA with Tukey post-test, $p = 0.16$, $p = 0.11$) (Fig 4H). This was likely due to the limit in statistical power with only 2 replicates. However, it was notable that for cells within Cluster 0, there was a significantly higher expression level for MHC II genes (*H2-Aa*, *H2-DMb1*, and *Cd74*) for coMtb cells compared to control or scBCG cells (Fig 4J). This suggests that coMtb might be able to elicit more mature or activated DCs in the airway. Overall, scRNAseq analysis shows that *Mycobacterium* exposure leads to minimal changes in T cell and dendritic cell populations in the airway, although we hypothesize that small changes in DC maturation/activation could have important impacts on adaptive immune priming dynamics after aerosol infection.

Cell-intrinsic remodeling of alveolar macrophages following *Mycobacterium* exposure licenses an interferon response *in vitro*

Analysis of the AM response to Mtb *in vivo* demonstrates that the very earliest immune response to Mtb is altered by previous *Mycobacterium* exposure. However, one limitation to this approach is the inability to discern whether changes to AMs are cell-intrinsic or dependent on the altered tissue environment, especially the presence of Mtb-specific T cells. Therefore, to determine whether *Mycobacterium* exposure induces cell-intrinsic changes to AMs, we isolated AMs from control, scBCG, and coMtb mice, stimulated them *ex vivo* with LPS, Pam3Cys, or H37Rv, and measured their transcriptional profiles 6 hours later (Fig 5A). First, PAMP-specific trends were notable. AMs from coMtb and scBCG mice showed distinct responses compared to AMs from control mice following LPS and H37Rv stimulation, but only minimal changes following Pam3Cys stimulation (Fig 5B and S3 Table). No obvious changes in innate receptor or adaptor expression explain the PAMP-specific differences (S11 Fig). Second, as we have previously reported, Mtb-infected AMs did not strongly up-regulate Nrf2-associated genes *ex vivo* (Fig 5C). Third, when we examined the gene sets that distinguished the *in vivo* AM response between scBCG and coMtb mice, “Interferon Alpha/Gamma Response” and “IL6 JAK STAT3” (Fig 2E), we found that the differences between exposure modalities were diminished *ex vivo*, suggesting contribution of the lung environment to the quality of the response (Fig 5C). Using Gene Set Enrichment Analysis, we identified “Interferon Gamma Response”, “Interferon Alpha Response”, “TNF α signaling via NF- κ B”, and “Inflammatory Response” pathways as the most strongly enriched for LPS and H37Rv responses from scBCG and coMtb AMs (Fig 5D). To assess whether the cell-intrinsic changes observed were long-lasting, we compared the responses of AMs at 8 or 23 weeks following scBCG vaccination by RT-qPCR. Increases in gene expression were as robust or even enhanced 23 weeks following exposure compared to 8 weeks, suggesting that exposure-induced changes to AMs are relatively long-lived (S12 Fig). To validate whether changes in gene expression were reflected at

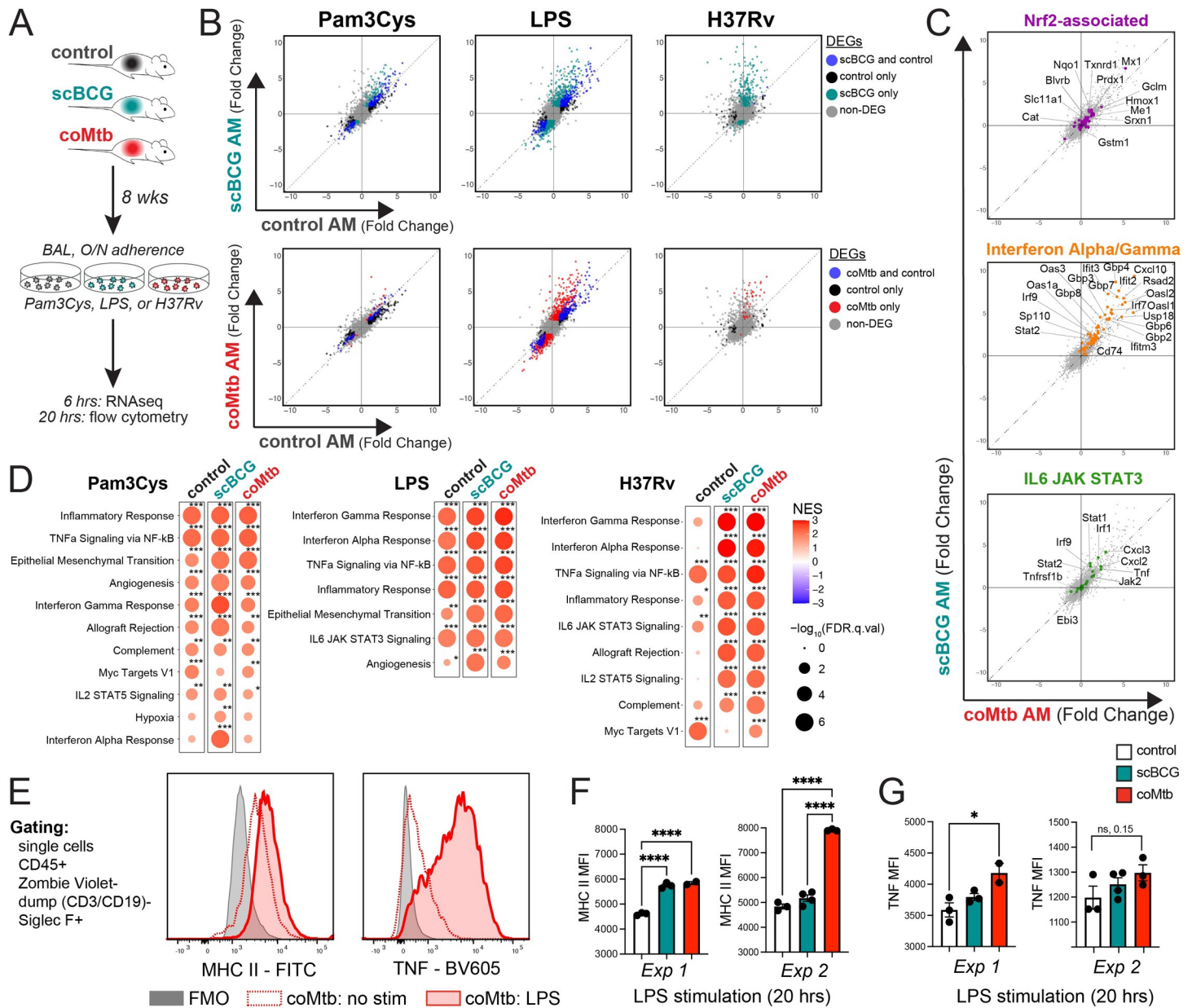


Fig 5. Cell-intrinsic remodeling of alveolar macrophages following *Mycobacterium* exposure. A) AM isolation 8 weeks following scBCG or coMtb exposure. AMs were stimulated with Pam3Cys (10 ng/ml), LPS (10 ng/ml), and H37Rv (effective MOI ~2:1) for 6 hours (RNA-seq) or 20 hours (flow cytometry). B-D) Gene expression changes measured by bulk RNA-seq for stimulated AMs compared to respective unstimulated AMs (i.e., LPS-stim control AM vs unstim control AM; LPS-stim scBCG AM vs unstim scBCG AM; LPS-stim coMtb AM vs unstim coMtb AM). B) Scatterplots, log₂ fold change gene expression for stimulated to unstimulated AMs for each condition (control, scBCG, coMtb). Differentially expressed genes (DEG) are highlighted for one or both conditions (|Fold change| > 2, FDR < 0.05 for Pam3Cys and LPS; |Fold change| > 2, FDR < 0.2 for H37Rv). C) Scatterplots, log₂ fold change gene expression for H37Rv-stimulated to unstimulated scBCG versus coMtb AMs. Genes highlighted derived from gene sets in Fig 2E. Nrf2-associated genes (56 genes, purple), Interferon Alpha/ Gamma Response (61 genes, orange), and IL6 JAK STAT3 (23 genes, green). D) Gene Set Enrichment Analysis results for 50 HALLMARK pathways. Pathways shown have NES > 1.5 and FDR < 0.05 for at least one of the conditions. *FDR < 0.05, **FDR < 0.01, ***FDR < 0.001. E) Gating strategy and MHC II and TNF histograms for coMtb AMs, no stimulation versus LPS. F-G) MHC II and TNF MFI in control, scBCG, and coMtb AMs after 20 hours of LPS stimulation. *p < 0.05, **p < 0.01, ***p < 0.001, One-way ANOVA with Tukey post-test.

<https://doi.org/10.1371/journal.ppat.1011871.g005>

the protein level, we sought to develop a flow cytometry-based assay to assess AM-specific responses. Primary AMs were stimulated with LPS for 20 hours and both MHC II and TNF expression were measured by flow cytometry (Fig 5E). We found that AM from coMtb mice

had significantly higher MHC II expression than controls and a similar pattern was seen for scBCG AM in 1 of 2 experiments (Fig 5F). AMs from coMtb mice also showed a significant increase in TNF expression in 1 of 2 experiments (Fig 5G).

Because the “Interferon Alpha Response” and “Interferon Gamma Response” pathways were most highly enriched for the H37Rv stimulation following *Mycobacterium* exposure, we decided to further investigate the Interferon-associated response [30]. We specifically sought out a dataset that would identify ISGs specific to Mtb-infected macrophages. To generate an IFN γ -derived signature, we would need a macrophage-T cell co-culture system and to sort out the Mtb-infected macrophages, because murine macrophages do not produce IFN γ during Mtb infection *in vitro*. Therefore, we decided to examine an IFN α/β -derived signature from a data set of Mtb-infected IFNAR $^{-/-}$ bone marrow derived macrophages (BMDMs). We categorized the macrophage response to H37Rv stimulation as “IFN-dependent” or “IFN-independent” based on gene expression of WT versus IFNAR $^{-/-}$ BMDMs following H37Rv infection (see methods section) (S4 Table) [38]. Expression of IFN-dependent genes was minimally induced in control AMs but strongly up-regulated in AMs from *Mycobacterium* exposed mice, as measured by the GSEA normalized enrichment score (NES) (Fig 6A, left). In contrast, expression of IFN-independent genes was modestly upregulated in control AMs and only slightly altered by *Mycobacterium* exposure (Fig 6A, right). When we applied these two gene sets to the *in vivo* response profiles described in Fig 2 generated for Mtb-infected AMs following high dose infection with mEmerald-H37Rv, we observe that Mtb-infected AMs from scBCG mice up-regulate the IFN-dependent response *in vivo*, suggesting that the licensing of the IFN-dependent response plays a role *in vivo* following BCG vaccination (Fig 6B). The difference between the *in vitro* and *in vivo* response for AMs from coMtb mice points to an additional contribution of the lung environment.

These results demonstrate that prior *Mycobacterium* exposure leads to cell-intrinsic changes in AMs that license an enhancement of IFN-dependent responses to Mtb that are retained *in vitro*, while qualitative differences in the response between scBCG and coMtb *in vivo* are dependent on signals from the lung environment.

Discussion

Here we describe remodeling of AMs, long-lived airway-resident innate cells, following two modalities of *Mycobacterium* exposure, scBCG vaccination and coMtb, a model of contained Mtb infection. AMs are the first cells to be productively infected in the lung following aerosol Mtb infection [10,11]. We previously showed that AMs initially respond to Mtb infection with a cell-protective, Nrf2-driven program that is detrimental to early host control [10], suggesting that the lack of a robust response by AMs prevents effective host control early on. In line with this model, others have shown that depletion of AMs or strategies that “bypass” AMs including directly injecting antigen-primed DCs or activating DCs accelerate the immune response and reduce bacterial burden [17,39,40]. However, how vaccination or prior exposures impact the initial response of AMs and whether there are therapeutic strategies that would enhance their initial response to infection have not been well studied [41].

Most studies examining the impacts of prior exposure to either Mtb or other species of mycobacteria, including BCG vaccination, have focused on the durable antigen-specific changes to the adaptive immune response. In contrast, we focused on changes to tissue-resident innate cells and their responses at the earliest stages of infection (≤ 14 days). Along with early changes to the T cell response, both scBCG and coMtb accelerate innate cell activation and immune cell recruitment in the first 10–14 days following Mtb aerosol infection, and even the very initial AM response to Mtb, within the first 24 hours of infection, is remodeled

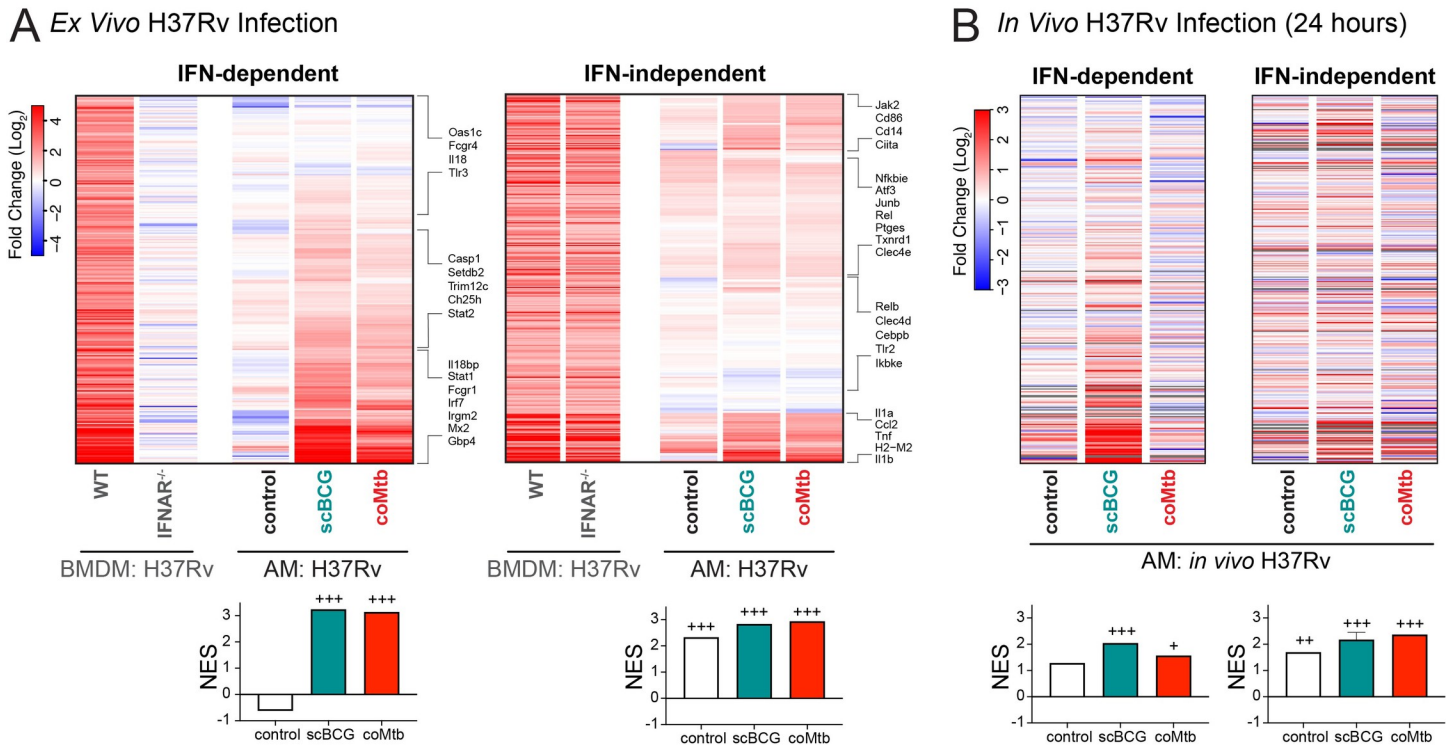


Fig 6. *Mycobacterium* exposure licenses an interferon-dependent response to H37Rv by alveolar macrophages. Gene expression changes measured by bulk RNA-seq for Mtb-infected AMs compared to respective unstimulated AMs (i.e., Mtb-inf control AM vs unstim control AM; Mtb-inf scBCG AM vs unstim scBCG AM; Mtb-inf coMtb AM vs unstim coMtb AM). A) Gene expression for control, scBCG, and coMtb AMs, 6 hour H37Rv infection *ex vivo*, log₂ fold change (Mtb-infected/uninfected). IFN-dependent genes (339 total) and IFN-independent genes (352 total) based on WT vs IFNAR^{-/-} BMDM bulk RNA-seq dataset (Olson et al, 2021) (see [Methods](#) section). B) Gene expression for control, scBCG, and coMtb AMs, 24 hour *in vivo* H37Rv infection, Mtb-infected sorted, log₂ fold change (Mtb-infected/uninfected) for the same IFN-dependent and IFN-independent gene sets in (A). Grey bars indicate N.D. Normalized Enrichment Score (NES) calculated by GSEA for two data sets alongside Hallmark Pathways. +FDR < 0.05, ++FDR < 0.01, +++FDR < 0.001.

<https://doi.org/10.1371/journal.ppat.1011871.g006>

following exposure to *Mycobacterium*. The durable changes observed fit with a number of recent studies which have uncovered either enhanced AM antimicrobial phenotypes [7–9] or impaired responses [42,43] following viral infection. Other studies have identified long-lasting changes to AMs following intranasal immunization of either adenoviral-based or inactivated whole cell vaccines [18,44,45].

We observe that the most robust cell-intrinsic changes to AM responses following scBCG or coMtb are found in IFN-dependent genes (Fig 6) and ISGs (Fig 2D), suggesting a critical role for interferon signaling in the changes to the early innate response in the lung during infection. Notably, this finding is not limited to the murine model. BAL from NHPs following IV, ID, or aerosol BCG vaccination similarly show AMs enriched for Interferon Gamma Response pathway genes [46]. AMs can respond to both Type I (IFN α/β) and Type II Interferons (IFN γ) and it is not possible to distinguish between responses to IFN α/β and IFN γ based on transcriptional analysis alone. The presence of live bacteria within both scBCG and coMtb models limits system-wide perturbations, such as T cell depletion or anti-IFN γ blockade, which would reverse containment [24]. For this reason, we have not been able to directly test how interferon signals derived from scBCG or coMtb remodel AMs in a cell-autonomous manner, but we envision future studies to examine the specific effects of individual cytokines on AM remodeling.

Even though IFNAR^{-/-} macrophages were used to generate the ISG signature identified in Fig 6, IFN γ is the more likely candidate to contribute to AM remodeling following *Mycobacterium* exposure. IFN γ is required for the generation of trained immunity in bone marrow-derived myeloid cells following IV BCG vaccination [15,47]. While IV and aerosol H37Rv infection was found to induce Type I IFNs and reduce myelopoiesis [47], we previously found that coMtb, in which Mtb is contained within the ear-draining lymph node, leads to low-level systemic cytokinemia, including IFN γ production. Using WT:Ifngr1^{-/-} mixed bone marrow chimeras, we showed that IFN γ signaling was responsible for monocyte and AM activation following establishment of coMtb [25]. Additionally, several reports have identified T cell-derived IFN γ as critical for altering AM function, although the immunological outcome varies substantially based on the context. In one study, T cell-derived IFN γ following adenoviral infection leads to AM activation, innate training and protection from *S. pneumoniae* [8], while in another study influenza-induced T cell-derived IFN γ leads to AM dysfunction and impaired clearance of *S. pneumoniae* [43]. A study of 88 SARS-CoV-2 patients identified AMs and T cell-derived IFN γ as part of a positive feedback loop in the airway [48]. In contrast, type I IFN signatures are associated with active TB or TB disease progression in both humans and non-human primates [49–51]. Host perturbations such as treatment with poly I:C or viral co-infection that induce type I IFN lead to worsened disease [52,53], type I IFN has been shown to block production of IL-1 β in myeloid cells during Mtb infection [54], and type I IFN drives mitochondrial stress and metabolic dysfunction in Mtb infected macrophages [38].

We note that the two modalities tested here consist of different mycobacterial species, different doses, and different routes. We expect that all three of these factors likely contribute to the quality of AM remodeling. For example, they could be important for the location, timing, and amount of IFN γ that AMs are exposed to. While an in-depth examination of each of these factors is beyond the scope of this study, the side-by-side comparison of the two different exposure models, scBCG and coMtb, allows us to examine the plasticity of AM phenotypes and the impact of the local and/or systemic environments leading to different responses. It is notable that scBCG is quickly cleared from WT mice, while coMtb replication is sustained in the superficial cervical lymph node for up to a year or longer [25]. Protection from H37Rv challenge mediated by coMtb is abrogated following antibiotic treatment but not completely lost [25]. This suggests that there may be different contributions to AM remodeling from active bacterial replication and from long-term microenvironment changes following bacterial clearance, which will be addressed in follow-up studies.

In particular, it is notable that the modality-specific signatures identified through *in vivo* transcriptional analysis disappeared following *ex vivo* isolation, along with the Nrf2 signature. The difference between *in vivo* and *ex vivo* signatures suggests a critical contribution of the altered lung microenvironments in AM remodeling, which deserves additional follow-up studies.

One additional limitation of our approach is that the *ex vivo* samples were collected in bulk, in the absence of cell sorting, and so, unlike the *in vivo* studies, a very small number of bystander AMs were likely collected alongside the Mtb-infected AMs, which could have had minor impacts on the transcriptional signatures. The fact that AMs can be remodeled into more than one state suggests additional complexity in innate immune features that has not yet been fully explored. Heterogeneity in myeloid reprogramming is not limited to the murine model and has also been observed in human monocytes [55].

Several studies have recently described innate-adaptive interactions within the airway that are thought to impact infection dynamics [46,48]. We note that in these models we observe innate cell activation and recruitment occurring at the same time as T cell activation and recruitment, and that these events are likely promoting one another. We are particularly

intrigued by the changes in AM MHC class II expression that we observed *in vivo* during the first two weeks of infection (Fig 1A) and following *ex vivo* stimulation (Fig 5F). AMs are considered to be poor antigen presenters, relative to other myeloid subsets, yet the faster Mtb-specific T cells are recruited to the lung, the more likely it is that AMs will serve as primary T cell targets [37,56–60]. Our results suggest that enhancement of AM antigen presentation could be one innate mechanism that could be targeted to complement and synergize with the adaptive immune response during infection. Other potential mechanisms by which AM remodeling may contribute to enhanced bacterial control after Mtb aerosol challenge include enhanced phagocytic activity or increased direct antimycobacterial activity, as previously demonstrated by Jeyanathan et al [19]. Future studies are needed to further interrogate the contribution of these innate mechanisms.

There are many other remaining questions. While we identify both cell-intrinsic changes and changes dependent on the lung environment, we do not yet know whether the cell-intrinsic changes are retained long-term in the absence of environmental cues. We do not know the durability of the changes, both cell-intrinsic and environment-dependent, and whether they are mediated by epigenetic effects. Our longest experiment showed retention of cell-intrinsic changes to AMs after 23 weeks. In Nemeth et al, we showed that antibiotic treatment lessened the protection mediated by coMtb, suggesting that ongoing replication is a key part of host protection [25]. AM remodeling is retained 8 weeks or longer after the initial exposures, a timepoint when there is little to no detectable mycobacteria in the lung, ruling out a requirement for local ongoing bacterial replication in AM remodeling, although systemic signals derived from remote bacterial replication may still play a role. We also performed several of these studies with intravenous BCG vaccination (ivBCG), which in the mouse model leads to more sustained bacterial replication than scBCG [61]. While we observed similar remodeling to AMs in the ivBCG model, these were not different in quality to those of scBCG vaccination, despite the major differences in bacterial replication and far greater T cell recruitment to the airway, suggesting that these changes are not required for AM remodeling (S9 Fig).

There is still much unknown about the signals that drive reprogramming of tissue-resident innate cells. Ideally, vaccines would be designed to leverage these signals in order to promote the most effective interactions between innate and adaptive responses. Identifying the ways that AMs are reprogrammed by inflammatory signals and the effects of their changed phenotypes on the early stages of infection will help to improve future vaccines or host-directed therapies.

Materials and methods

Ethics statement

Animal studies performed at Seattle Children's Research Institute were performed in compliance with and approval by the Seattle Children's Research Institute's Institutional Animal Care and Use Committee. Animal studies performed at University of Massachusetts Amherst were performed in compliance with and approval by the University of Massachusetts Amherst's Institutional Animal Care and Use Committee. All mice were housed and maintained in specific pathogen-free conditions.

Mice

C57BL/6 mice were purchased from Jackson Laboratories (Bar Harbor, ME). 6–12 week old male and female mice were used for all experiments, except for RNA-sequencing, which used only female mice for uniformity. Mice infected with Mtb were housed in Biosafety Level 3 facilities in Animal Biohazard Containment Suites.

Mycobacteria exposure models: BCG immunization and establishment of coMtb

BCG-Pasteur was cultured in Middlebrook 7H9 broth at 37°C to an OD of 0.1–0.3. Bacteria was diluted in PBS and 1 x 10⁶ CFU in 200 ml was injected subcutaneous (SC) or intravenous (IV). Intradermal infections to establish coMtb were performed as formerly described [24], with some modifications as detailed previously [25]. Briefly, 10,000 CFU of Mtb (H37Rv) in logarithmic phase growth were injected intradermally into the ear in 10 µL PBS using a 10 µL Hamilton Syringe, following anesthesia with ketamine/xylazine.

***M. tuberculosis* aerosol infections and lung mononuclear cell isolation**

Aerosol infections were performed with wildtype H37Rv, including some transformed with an mEmerald reporter pMV261 plasmid, generously provided by Dr. Chris Sassetti and Christina Baer (University of Massachusetts Medical School, Worcester, MA). For both standard (~100 CFU) and high dose (1,473–4,800 CFU) infections, mice were enclosed in an aerosol infection chamber (Glas-Col) and frozen stocks of bacteria were thawed and placed inside the associated nebulizer. To determine the infectious dose, three mice in each infection were sacrificed one day later and lung homogenates were plated onto 7H10 plates for CFU enumeration. High dose challenge and sorting of Mtb-infected AM was performed 4 weeks following scBCG vaccination and 2 weeks following coMtb vaccination as previously described [62]. All other analysis was performed 8 weeks following *Mycobacterium* exposures.

Lung single cell suspensions

At each time point, lungs were removed, and single-cell suspensions of lung mononuclear cells were prepared by Liberase Blendzyme 3 (70 µg/ml, Roche) digestion containing DNaseI (30 µg/ml; Sigma-Aldrich) for 30 mins at 37°C and mechanical disruption using a gentleMACS dissociator (Miltenyi Biotec), followed by filtering through a 70 µm cell strainer. Cells were resuspended in FACS buffer (PBS, 1% FBS, and 0.1% NaN₃) prior to staining for flow cytometry. For bacterial enumeration, lungs were processed in 0.05% Tween-80 in PBS using a gentleMACS dissociator (Miltenyi Biotec) and were plated onto 7H10 plates for CFU enumeration. Δ CFU (log) was calculated as follows: Δ CFU = log((sample CFU)/(average control CFU*)). *For respective experiment, timepoint, and organ. A Δ CFU value of -1 corresponds to a 10-fold reduction in CFU for the sample, compared to the control. Similarly, a Δ CFU value of 1 corresponds to a 10-fold increase in CFU.

Alveolar macrophage isolation

AMs for cell sorting, bulk RNA-sequencing, single cell RNA-sequencing, and *ex vivo* stimulation were collected by bronchoalveolar lavage (BAL). BAL was performed by exposing the trachea of euthanized mice, puncturing the trachea with Vannas Micro Scissors (VWR) and injecting 1 mL PBS using a 20G-1" IV catheter (McKesson) connected to a 1 mL syringe. The PBS was flushed into the lung and then aspirated three times and the recovered fluid was placed in a 15mL tube on ice. The wash was repeated 3 additional times. Cells were filtered and spun down. For antibody staining, cells were suspended in FACS buffer. For cell culture, cells were plated at a density of 5 x 10⁴ cells/well (96-well plate) in complete RPMI (RPMI plus FBS (10%, VWR), L-glutamine (2mM, Invitrogen), and Penicillin-Streptomycin (100 U/ml; Invitrogen) and allowed to adhere overnight in a 37°C humidified incubator (5% CO₂). Media with antibiotics were washed out prior to infection with Mtb.

Cell sorting and flow cytometry

Fc receptors were blocked with anti-CD16/32 (2.4G2, BD Pharmingen). Cell viability was assessed using Zombie Violet dye (Biolegend). Cells were suspended in 1X PBS (pH 7.4) containing 0.01% NaN₃ and 1% fetal bovine serum (i.e., FACS buffer). Surface staining, performed at 4 degrees for 20 minutes, included antibodies specific for murine: Siglec F (E50-2440, BD Pharmingen), CD11b (M1/70), CD64 (X54-5/7.1), CD45 (104), CD3 (17A2, eBiosciences), CD19 (1D3, eBiosciences), CD11c (N418), I-A/I-E (M5/114.15.2), Ly6G (1A8), Ly6C (HK1.4), TNF (MP6-XT22). For ICS, Brefeldin A was added for duration of LPS stimulation. Cyto-Fast Fix/Perm and Cyto-Fast Perm Wash reagents were used for intracellular staining. Reagents are from Biolegend unless otherwise noted. MHC class II tetramers ESAT-6 (I-A(b) 4–17, sequence: QQWNFAGIEAAASA) and MHC class I tetramers TB10.4 (H-2K(b) 4–11, sequence: IMYNYPAM) were obtained from the National Institutes of Health Tetramer Core Facility. Cell sorting was performed on a FACS Aria (BD Biosciences). Sorted cells were collected in complete media, spun down, resuspended in TRIzol, and frozen at -80°C overnight prior to RNA isolation. Samples for flow cytometry were fixed in 2% paraformaldehyde solution in PBS and analyzed using a LSRII flow cytometer (BD Biosciences) and FlowJo software (Tree Star, Inc.).

Bulk RNA-sequencing and analysis

All high dose infections and sorting for bulk RNA-sequencing of Mtb-infected AMs (control, scBCG, and coMtb) were performed in the ABSL-3 facility at Seattle Children's Research Institute. All infections used the same Mtb strain, mEmerald-H37Rv, and the TRIzol-based RNA isolation protocol was performed by the same individual (D.M.). RNA isolation was performed using TRIzol (Invitrogen), two sequential chloroform extractions, Glycoblue carrier (Thermo Fisher), isopropanol precipitation, and washes with 75% ethanol. RNA was quantified with the Bioanalyzer RNA 6000 Pico Kit (Agilent). cDNA libraries were constructed using the SMARTer Stranded Total RNA-Seq Kit (v2)–Pico Input Mammalian (Clontech) following the manufacturer's instructions. Libraries were amplified and then sequenced on an Illumina NextSeq (2 x 76, paired-end (sorted BAL cells) or 2 x 151, paired-end (ex vivo stimulation samples)). Stranded paired-end reads were preprocessed: The first three nucleotides of R2 were removed as described in the SMARTer Stranded Total RNA-Seq Kit–Pico Input Mammalian User Manual (v2: 063017) and read ends consisting of more than 66% of the same nucleotide were removed. The remaining read pairs were aligned to the mouse genome (mm10) + Mtb H37Rv genome using the gsnap aligner [63] (v. 2018-07-04) allowing for novel splicing. Concordantly mapping read pairs (~20 million / sample) that aligned uniquely were assigned to exons using the iocond program and gene definitions from Ensembl Mus_Musculus GRCm38.78 coding and non-coding genes. Genes with low expression were filtered using the “filterByExpr” function in the edgeR package [64]. Differential expression was calculated using the “edgeR” package [64] from ioconductor.org. False discovery rate was computed with the Benjamini-Hochberg algorithm. Hierarchical clusterings were performed in R using ‘Tscust’ and ‘hclust’ libraries. Heat map and scatterplot visualizations were generated in R using the ‘heatmap.2’ and ‘ggplot2’ libraries, respectively.

Gene Set Enrichment Analysis (GSEA)

Input data for GSEA consisted of lists, ranked by $-\log(p\text{-value})$, comparing RNAseq expression measures of target samples and naïve controls including directionality of fold-change. Mouse orthologs of human Hallmark genes were defined using a list provided by Molecular Signatures Database (MsigDB) [65]. GSEA software was used to calculate enrichment of ranked lists

in each of the respective hallmark gene lists, as described previously [66]. A nominal p-value for each ES is calculated based on the null distribution of 1,000 random permutations. To correct for multiple hypothesis testing, a normalized enrichment score (NES) is calculated that corrects the ES based on the null distribution. A false-discovery rate (FDR) is calculated for each NES. Leading edge subsets are defined as the genes in a particular gene set that are part of the ranked list at or before the running sum reaches its maximum value.

Ingenuity Pathway Analysis (IPA)

IPA (QIAGEN) was used to identify enriched pathways for differentially expressed genes between naïve and Mtb-infected AMs (cut-off values: FDR < 0.01, |FC| > 2). The top 20 canonical pathways with enrichment score p-value < 0.05 with greater than 10 gene members are reported.

Single cell RNA-sequencing

BAL from 10 mice per condition was pooled for each sample, with two independent replicates per condition. Samples were prepared for methanol fixation following protocol “CG000136 Rev. D” from 10X Genomics [67]. Briefly, samples were filtered with 70 µm filters and red blood cells were lysed with ACK lysis buffer. Samples were resuspended in 1 mL ice-cold DPBS using a wide-bore tip and transferred to a 1.5 mL low-bind Eppendorf tube. Samples were centrifuged at $700 \times g$ for 5 minutes at 4°C. Supernatant was carefully removed with a p1000 pipette, and the cell pellet was washed two more times with DPBS, counted, and resuspended in 200 µL ice-cold DPBS/ 1×10^6 cells. 800 µL of ice-cold methanol was added dropwise for a final concentration of 80% methanol. Samples were incubated at -20°C for 30 minutes and then stored at -80°C for up to 6 weeks prior to rehydration. For rehydration, frozen samples were equilibrated to 4°C, centrifuged at $1,000 \times g$ for 10 minutes at 4°C, and resuspended in 50 µL of Wash-Resuspension Buffer (0.04% BSA + 1mM DTT + 0.2U/µL Protector RNAase Inhibitor in 3× SSC buffer) to achieve ~1,000 cells/µL (assuming 75% sample loss).

Single cell RNA-sequencing analysis

Libraries were prepared using the Next GEM Single Cell 3' Reagent Kits v3.1 (Dual Index) (10X Genomics) following the manufacturer's instructions. Raw sequencing data were aligned to the mouse genome (mm10) and UMI counts determined using the Cell Ranger pipeline (10X Genomics). Data processing, integration, and analysis was performed with Seurat v.3 [68]. Droplets containing less than 200 detected genes, more than 4000 detected genes (doublet discrimination), or more than 5% mitochondrial were discarded. Genes expressed by less than 3 cells across all samples were removed. Unbiased annotation of clusters using the Immgen database [69] as a reference was performed with “SingleR” package [70]. Pseudotime analysis was performed using the “SeuratWrappers” and “Monocle3” R packages [71]. Data visualization was performed with the “Seurat”, “tidyverse”, “cowplot”, and “viridis” R packages.

Alveolar macrophage *Ex Vivo* stimulation

AMs were isolated by bronchoalveolar lavage and pooled from 5 mice per group. Cells were plated at a density of 5×10^4 cells/well (96-well plate) in complete RPMI (RPMI plus FBS (10%, VWR), L-glutamine (2mM, Invitrogen), and Penicillin-Streptomycin (100 U/ml; Invitrogen) and allowed to adhere overnight in a 37°C humidified incubator (5% CO₂). Media with antibiotics and non-adherent cells were washed out prior to stimulation. AM were stimulated with LPS (LPS from Salmonella Minnesota, List Biologicals, #R595, 10 ng/ml), Pam3Cys

(Pam3CSK4, EMC Microcollections, GmbH, 10 ng/ml), or H37Rv (effective MOI ~2:1). H37Rv was prepared by culturing from frozen stock in 7H9 media at 37°C for 48 hours to O.D. of 0.1–0.3. The final concentration was calculated based on strain titer and bacteria was added to macrophages for two hours. Cultures were then washed three times to remove extracellular bacteria. Cell cultures were washed once in PBS after 6 hours to remove dead cells and collected in TRIzol for RNA isolation via chloroform/isopropanol extraction or collected after 20 hours for flow cytometry and ICS.

Filtering for IFN dependent and independent gene sets

“IFN dependent” and “IFN independent” gene sets were generated from data from Olson et al [38], using the following filters starting from a total of 1,233 genes up-regulated in H37Rv-stimulated WT BMDM with average CPM >1, log₂ fold change > 1 and FDR < 0.01:

“IFN dependent” = H37Rv-stimulated IFNAR^{-/-} BMDM: log₂ fold change < 1 AND H37Rv-stimulated WT vs IFNAR^{-/-}: log₂ fold change > 2 = **339 genes**

“IFN independent” = H37Rv-stimulated IFNAR^{-/-} BMDM: log₂ fold change > 1, FDR < 0.01 AND H37Rv-stimulated WT vs IFNAR^{-/-}: log₂ fold change < 2 = **352 genes**

qRT-PCR

Quantitative PCR reactions were carried out using TaqMan primer probes (ABI) and TaqMan Fast Universal PCR Master Mix (ThermoFisher) in a CFX384 Touch Real-Time PCR Detection System (BioRad). Data were normalized by the level of *Efla* expression in individual samples.

Statistical analyses

RNA-sequencing was analyzed using the edgeR package from [Bioconductor.org](https://bioconductor.org) and the false discovery rate was computed using the Benjamini-Hochberg algorithm. All other data are presented as mean ± SEM and analyzed by one-way ANOVA (95% confidence interval) with Tukey post-test (for comparison of multiple conditions). Statistical analysis and graphical representation of data was performed using either GraphPad Prism v6.0 software or R. PCA plots generated using “Prcomp” and “Biplot” packages. Venn diagrams and gene set intersection analysis was performed using Intervene [72]. p-values, * p < 0.05, ** p < 0.01, *** p < 0.001.

Supporting information

S1 Fig. (related to Fig 1). Flow cytometry gating schemes. Gating strategies for myeloid (A) and T cell (B) analysis.
(TIF)

S2 Fig. (related to Fig 1). *Mycobacterium* exposure provides protection against standard low-dose H37Rv aerosol challenge. A) Lung, spleen, and lung-draining lymph node (LN) CFU in control mice at deposition, days 10, 12, 14, and 28. B-E) Summary plots of ΔCFU (log) in lung, spleen, and LN following low-dose infection with H37Rv at day 10 (B), day 12 (C), day 14 (D), and day 28 (E). *p < 0.05, **p < 0.01, ***p < 0.001. One-way ANOVA with Tukey post-test. Data compiled from 2–3 independent experiments per condition, with 5 mice per group for each experiment.
(TIF)

S3 Fig. (related to Fig 2). Top 20 Canonical Pathways by Ingenuity Pathway Analysis for up-regulated genes by Mtb-infected alveolar macrophages. IPA analysis for Mtb-infected AMs from control, scBCG, and coMtb mice 24 hours following high dose mEmerald-H37Rv infection. Data representative of 3 independent experiments per condition. (TIF)

S4 Fig. (related to Fig 2). Transcriptional changes to naïve alveolar macrophages following *Mycobacterium* exposure by bulk RNA-sequencing. Bulk RNA-seq profiles of naïve AMs (isolated alongside Mtb-infected AMs). Gene expression changes within naïve AMs are compared to AMs from control mice: naïve scBCG AM vs naïve control AM; naïve coMtb AM vs naïve control AM. A-B) Volcano plots depicting changes in baseline gene expression of naïve AMs from scBCG (A) and coMtb(B) mice compared to naïve AMs from control mice. Significantly changed genes ($FDR < 0.05$, $|FC| > 2$) highlighted and labeled. C) Gene expression for innate receptors and adaptors of interest, \log_2 fold change, unstimulated AMs from scBCG and coMtb mice compared to unstimulated AMs from control mice. * $FDR < 0.01$. Compiled from 2 independent experiments for each condition. (TIF)

S5 Fig. (related to Fig 3). Flow analysis of BAL samples prepared for 10X single-cell RNA-sequencing. Percentage of each population (AM, lymphocytes, eosinophils, MDM, other $CD45^+$) out of $CD45^+$ ZV. AM = Siglec F^+ $CD64^+$, Eosinophils = Siglec F^+ $CD64^-$, lymphocytes = $CD3/CD19^+$, MDM = Siglec F^- $CD64^+$, other $CD45^+$ = $CD3^-$ $CD19^-$ Siglec F^- $CD64^-$. Note: One of the two coMtb samples analyzed by flow cytometry did not have an accompanying 10X sample. The second coMtb 10X sample was processed separately without flow analysis. (TIF)

S6 Fig. (related to Fig 3). Top 10 genes differentially expressed for each of 11 macrophage subclusters. Heatmap of genes that are most differentially expressed for each of 11 clusters with all other clusters. Genes filtered with \log fold change threshold of > 0.25 and minimum percentage expression of 25% of cells. All genes but one (*Gsto1*) had an adjusted p-value of $< 1.0 \times 10^{-5}$. *Five genes (*Fabp4*, *Fabp5*, *Stmn1*, *Mki67*, *Cbr2*) met this criterion for more than one cluster, grouped with the more abundant cluster. Data is compiled from two independent experiments, 3 conditions each, for a total of 6 samples. (TIF)

S7 Fig. (related to Fig 3). UMAP gene expression plots for genes associated with macrophage subcluster 3 and found in AM_2 (Pisu et al) (31). Genes associated with mitochondrial oxidative phosphorylation (*mt-Co1*, *mt-Cytb*, *mt-Nd2*), chromatin remodeling (*Ankrd11*, *Baz1a*), macrophage-associated transcription factors (*Cebpb*, *Zeb2*, *Bhlhe40*, *Hif1a*), and CARD9 signaling (*Malt1*, *Bcl10*). Data is compiled from two independent experiments with 3 conditions each, for a total of 6 samples. (TIF)

S8 Fig. (related to Fig 3). Frequency and gene expression of Cluster 6 macrophages across exposure conditions. A) Single-cell RNA-sequencing from BAL samples from control, scBCG, and coMtb mice. Subcluster of macrophages with each cluster annotated. Relative frequency of Cluster 6 for each replicate. B) Differentially expressed genes within Cluster 6 between control vs scBCG vs coMtb samples. Wilcoxon Rank Sum Test, Bonferroni adjusted p-value, ***adj-p < 0.001 . (TIF)

S9 Fig. (related to Fig 3). IV BCG vaccination leads to similar remodeling of alveolar macrophages as SC BCG vaccination. A-B) Bulk RNA-seq gene expression analysis between naive and Mtb-infected AMs 24 hours following high-dose mEmerald-H37Rv infection in mice previously exposed to scBCG, ivBCG, and coMtb, compared to controls. (controls- reported in Rothchild et al, 2019(10); CMTB- reported in Nemeth et al, 2020(25)). A) Principal Component Analysis using DEG (fold change > |2|, FDR < 0.05) in Mtb-infected AMs at 24 hours. B) Heatmap of 131 DEG at 24 hours in Mtb-infected AM (left), Interferon Stimulated Genes, derived from macrophage response to IFN α (fold change >2, p-value < 0.01) Mostafavi et al, 2016 (30)(middle), IL6 JAK STAT3 hallmark pathway (right). C) Relative frequency of 3 key clusters for macrophage subset from control, scBCG, ivBCG, and coMtb scRNAseq BAL samples. (A-B) Compiled from 3+ independent experiments per condition for control, 2 independent experiments per condition for scBCG, ivBCG, and coMtb. (C) Data is compiled from two independent experiments (circle, triangle) with 3 conditions each for a total of 6 samples.

(TIF)

S10 Fig. (related to Fig 4). UMAP gene expression plots of cluster and lineage marker genes of interest for T cell subclusters. Data is compiled from two independent experiments with 3 conditions each for a total of 6 samples.

(TIF)

S11 Fig. (related to Fig 5). Gene expression of alveolar macrophages from *ex vivo* stimulations. A) Gene expression changes measured by bulk RNA-seq for stimulated AMs compared to respective unstimulated AMs (i.e., LPS-stim control AM vs unstim control AM; LPS-stim scBCG AM vs unstim scBCG AM; LPS-stim coMtb AM vs unstim coMtb AM). AMs were stimulated for 6 hours with Pam3Cys (10 ng/ml), LPS (10 ng/ml), or H37Rv (effective MOI ~2:1). Volcano plots depict fold change (\log_2) and P-value ($-\log_{10}$) for each stimulation condition for each of the three groups (control scBCG, coMtb) compared to the respective unstimulated controls. DEG (p-value < 0.001; |fold change| > 2) highlighted and labeled, space permitting. B) Baseline gene expression for innate receptors and adaptors of interest from scBCG and coMtb AM compared to control AM, \log_2 fold change, unstim scBCG AM vs unstim control AM; unstim coMtb AM vs unstim control AM. Compiled from 3 independent experiments.

(TIF)

S12 Fig. (related to Fig 5). Cell-intrinsic changes in alveolar macrophage response is retained 23 weeks following vaccination. Gene expression of *Mx1*, *Cxcl10*, *Il1b*, *Cxcl2*, *Irf7*, and *Il6* as measured by qPCR in AMs isolated by BAL from mice 8 and 23 weeks following scBCG vaccination and from age-matched controls, with and without LPS (10 ng/ml) stimulation. Data is representative of technical AM duplicates from a single experiment.

(TIF)

S1 Table. RNA-Sequencing data for alveolar macrophages 24 hours following high dose H37Rv-mEmerald challenge from scBCG mice.

(XLSX)

S2 Table. Top differentially expressed genes for individual clusters for macrophage, T cell, and dendritic cell sub-cluster analysis.

(XLSX)

S3 Table. RNA-Sequencing data for *ex vivo* stimulated alveolar macrophages.

(XLSX)

S4 Table. IFN-independent and IFN-dependent genes based on WT and IFNAR^{-/-} BMDM RNA-seq data.

(XLSX)

Acknowledgments

We thank the Animal Care staff at Seattle Children's Research Institute and University of Massachusetts Amherst, Pamela Troisch and the Next Gen Sequencing core at the Institute for Systems Biology. The authors acknowledge Research Scientific Computing at Seattle Children's Research Institute for providing HPC resources that have contributed to the research results reported within this paper. We thank members of the Aderem, Urdahl, and Rothchild labs for helpful discussions.

Author Contributions

Conceptualization: Dat Mai, Johannes Nemeth, Kevin Urdahl, Alan H. Diercks, Alan Aderem, Alissa C. Rothchild.

Data curation: Michael Morikubo, Alan H. Diercks, Alissa C. Rothchild.

Formal analysis: Dat Mai, Michael Morikubo, Alan H. Diercks, Alissa C. Rothchild.

Funding acquisition: Kevin Urdahl, Alan H. Diercks, Alan Aderem, Alissa C. Rothchild.

Investigation: Dat Mai, Ana Jahn, Tara Murray, Pamela N. Lim, Maritza M. Cervantes, Linh K. Pham, Alissa C. Rothchild.

Supervision: Alan H. Diercks, Alan Aderem, Alissa C. Rothchild.

Validation: Dat Mai, Alissa C. Rothchild.

Writing – original draft: Alan H. Diercks, Alissa C. Rothchild.

Writing – review & editing: Dat Mai, Pamela N. Lim, Linh K. Pham, Alan H. Diercks, Alissa C. Rothchild.

References

1. World Health Organization. Global tuberculosis report 2021. Geneva. Licence: CC BY-NC-SA 3.0 IGO. 2022.
2. Dheda K, Perumal T, Moultrie H, Perumal R, Esmail A, Scott AJ, et al. The intersecting pandemics of tuberculosis and COVID-19: population-level and patient-level impact, clinical presentation, and corrective interventions. *Lancet Respir Med*. 2022. [https://doi.org/10.1016/S2213-2600\(22\)00092-3](https://doi.org/10.1016/S2213-2600(22)00092-3) PMID: 35338841
3. Netea MG, Dominguez-Andres J, Barreiro LB, Chavakis T, Divangahi M, Fuchs E, et al. Defining trained immunity and its role in health and disease. *Nat Rev Immunol*. 2020; 20(6):375–88. <https://doi.org/10.1038/s41577-020-0285-6> PMID: 32132681
4. Sherwood ER, Burelbach KR, McBride MA, Stothers CL, Owen AM, Hernandez A, et al. Innate Immune Memory and the Host Response to Infection. *J Immunol*. 2022; 208(4):785–92. <https://doi.org/10.4049/jimmunol.2101058> PMID: 35115374
5. Khader SA, Divangahi M, Hanekom W, Hill PC, Maeurer M, Makar KW, et al. Targeting innate immunity for tuberculosis vaccination. *J Clin Invest*. 2019; 129(9):3482–91. <https://doi.org/10.1172/JCI128877> PMID: 31478909
6. Hoyer FF, Naxerova K, Schloss MJ, Hulsmans M, Nair AV, Dutta P, et al. Tissue-Specific Macrophage Responses to Remote Injury Impact the Outcome of Subsequent Local Immune Challenge. *Immunity*. 2019; 51(5):899–914 e7. <https://doi.org/10.1016/j.immuni.2019.10.010> PMID: 31732166

7. Aegerter H, Kulikauskaitė J, Crotta S, Patel H, Kelly G, Hessel EM, et al. Influenza-induced monocyte-derived alveolar macrophages confer prolonged antibacterial protection. *Nat Immunol.* 2020; 21(2):145–57. <https://doi.org/10.1038/s41590-019-0568-x> PMID: 31932810
8. Yao Y, Jeyanathan M, Haddadi S, Barra NG, Vaseghi-Shanjani M, Damjanovic D, et al. Induction of Autonomous Memory Alveolar Macrophages Requires T Cell Help and Is Critical to Trained Immunity. *Cell.* 2018; 175(6):1634–50 e17. <https://doi.org/10.1016/j.cell.2018.09.042> PMID: 30433869
9. Zhu B, Wu Y, Huang S, Zhang R, Son YM, Li C, et al. Uncoupling of macrophage inflammation from self-renewal modulates host recovery from respiratory viral infection. *Immunity.* 2021; 54(6):1200–18 e9. <https://doi.org/10.1016/j.immuni.2021.04.001> PMID: 33951416
10. Rothchild AC, Olson GS, Nemeth J, Amon LM, Mai D, Gold ES, et al. Alveolar macrophages generate a noncanonical NRF2-driven transcriptional response to *Mycobacterium tuberculosis* in vivo. *Sci Immunol.* 2019; 4(37). <https://doi.org/10.1126/sciimmunol.aaw6693> PMID: 31350281
11. Cohen SB, Gern BH, Delahaye JL, Adams KN, Plumlee CR, Winkler JK, et al. Alveolar Macrophages Provide an Early *Mycobacterium tuberculosis* Niche and Initiate Dissemination. *Cell Host Microbe.* 2018; 24(3):439–46 e4. <https://doi.org/10.1016/j.chom.2018.08.001> PMID: 30146391
12. Mangtani P, Abubakar I, Ariti C, Beynon R, Pimpin L, Fine PE, et al. Protection by BCG vaccine against tuberculosis: a systematic review of randomized controlled trials. *Clin Infect Dis.* 2014; 58(4):470–80. <https://doi.org/10.1093/cid/cit790> PMID: 24336911
13. Trunz BB, Fine P, Dye C. Effect of BCG vaccination on childhood tuberculous meningitis and miliary tuberculosis worldwide: a meta-analysis and assessment of cost-effectiveness. *Lancet.* 2006; 367(9517):1173–80. [https://doi.org/10.1016/S0140-6736\(06\)68507-3](https://doi.org/10.1016/S0140-6736(06)68507-3) PMID: 16616560
14. Lange C, Aaby P, Behr MA, Donald PR, Kaufmann SHE, Netea MG, et al. 100 years of *Mycobacterium bovis* bacille Calmette-Guerin. *Lancet Infect Dis.* 2022; 22(1):e2–e12.
15. Kaufmann E, Sanz J, Dunn JL, Khan N, Mendonca LE, Pacis A, et al. BCG Educates Hematopoietic Stem Cells to Generate Protective Innate Immunity against Tuberculosis. *Cell.* 2018; 172(1–2):176–90 e19. <https://doi.org/10.1016/j.cell.2017.12.031> PMID: 29328912
16. Delahaye JL, Gern BH, Cohen SB, Plumlee CR, Shafiani S, Gerner MY, et al. Cutting Edge: Bacillus Calmette-Guerin-Induced T Cells Shape *Mycobacterium tuberculosis* Infection before Reducing the Bacterial Burden. *J Immunol.* 2019; 203(4):807–12.
17. Das S, Marin ND, Esaulova E, Ahmed M, Swain A, Rosa BA, et al. Lung Epithelial Signaling Mediates Early Vaccine-Induced CD4(+) T Cell Activation and *Mycobacterium tuberculosis* Control. *mBio.* 2021; 12(4):e0146821. <https://doi.org/10.1128/mBio.01468-21> PMID: 34253059
18. Mata E, Tarancon R, Guerrero C, Moreo E, Moreau F, Uranga S, et al. Pulmonary BCG induces lung-resident macrophage activation and confers long-term protection against tuberculosis. *Sci Immunol.* 2021; 6(63):eabc2934. <https://doi.org/10.1126/sciimmunol.abc2934> PMID: 34559551
19. Jeyanathan M, Vaseghi-Shanjani M, Afkhami S, Grondin JA, Kang A, D'Agostino MR, et al. Parenteral BCG vaccine induces lung-resident memory macrophages and trained immunity via the gut-lung axis. *Nat Immunol.* 2022; 23(12):1687–702. <https://doi.org/10.1038/s41590-022-01354-4> PMID: 36456739
20. Arts RJW, Moorlag S, Novakovic B, Li Y, Wang SY, Oosting M, et al. BCG Vaccination Protects against Experimental Viral Infection in Humans through the Induction of Cytokines Associated with Trained Immunity. *Cell Host Microbe.* 2018; 23(1):89–100 e5. <https://doi.org/10.1016/j.chom.2017.12.010> PMID: 29324233
21. Kleinnijenhuis J, Quintin J, Preijers F, Joosten LA, Jacobs C, Xavier RJ, et al. BCG-induced trained immunity in NK cells: Role for non-specific protection to infection. *Clin Immunol.* 2014; 155(2):213–9. <https://doi.org/10.1016/j.clim.2014.10.005> PMID: 25451159
22. Koeken V, van der Pasch ES, Leijte GP, Mourits VP, de Bree LCJ, Moorlag S, et al. The effect of BCG vaccination on alveolar macrophages obtained from induced sputum from healthy volunteers. *Cytokine.* 2020; 133:155135. <https://doi.org/10.1016/j.cyto.2020.155135> PMID: 32534356
23. Soto JA, Galvez NMS, Andrade CA, Ramirez MA, Riedel CA, Kalergis AM, et al. BCG vaccination induces cross-protective immunity against pathogenic microorganisms. *Trends Immunol.* 2022; 43(4):322–35. <https://doi.org/10.1016/j.it.2021.12.006> PMID: 35074254
24. Kupz A, Zedler U, Staber M, Kaufmann SH. A Mouse Model of Latent Tuberculosis Infection to Study Intervention Strategies to Prevent Reactivation. *PLoS One.* 2016; 11(7):e0158849. <https://doi.org/10.1371/journal.pone.0158849> PMID: 27391012
25. Nemeth J, Olson GS, Rothchild AC, Jahn AN, Mai D, Duffy FJ, et al. Contained *Mycobacterium tuberculosis* infection induces concomitant and heterologous protection. *PLoS Pathog.* 2020; 16(7):e1008655. <https://doi.org/10.1371/journal.ppat.1008655> PMID: 32673357

26. Cadena AM, Hopkins FF, Maiello P, Carey AF, Wong EA, Martin CJ, et al. Concurrent infection with *Mycobacterium tuberculosis* confers robust protection against secondary infection in macaques. *PLoS Pathog*. 2018; 14(10):e1007305. <https://doi.org/10.1371/journal.ppat.1007305> PMID: 30312351
27. Andrews JR, Noubary F, Walensky RP, Cerda R, Losina E, Horsburgh CR. Risk of progression to active tuberculosis following reinfection with *Mycobacterium tuberculosis*. *Clin Infect Dis*. 2012; 54(6):784–91. <https://doi.org/10.1093/cid/cir951> PMID: 22267721
28. Wolf AJ, Linas B, Trevejo-Nunez GJ, Kincaid E, Tamura T, Takatsu K, et al. *Mycobacterium tuberculosis* infects dendritic cells with high frequency and impairs their function in vivo. *J Immunol*. 2007; 179(4):2509–19. <https://doi.org/10.4049/jimmunol.179.4.2509> PMID: 17675513
29. Mollenkopf HJ, Kursar M, Kaufmann SH. Immune response to postprimary tuberculosis in mice: *Mycobacterium tuberculosis* and *Mycobacterium bovis* bacille Calmette-Guerin induce equal protection. *J Infect Dis*. 2004; 190(3):588–97.
30. Mostafavi S, Yoshida H, Moodley D, LeBoite H, Rothamel K, Raj T, et al. Parsing the Interferon Transcriptional Network and Its Disease Associations. *Cell*. 2016; 164(3):564–78. <https://doi.org/10.1016/j.cell.2015.12.032> PMID: 26824662
31. Pisu D, Huang L, Narang V, Theriault M, Le-Bury G, Lee B, et al. Single cell analysis of *M. tuberculosis* phenotype and macrophage lineages in the infected lung. *J Exp Med*. 2021; 218(9). <https://doi.org/10.1084/jem.20210615> PMID: 34292313
32. Travaglini KJ, Nabhan AN, Penland L, Sinha R, Gillich A, Sit RV, et al. A molecular cell atlas of the human lung from single-cell RNA sequencing. *Nature*. 2020; 587(7835):619–25. <https://doi.org/10.1038/s41586-020-2922-4> PMID: 33208946
33. Scott CL, T'Jonck W, Martens L, Todorov H, Sichien D, Soen B, et al. The Transcription Factor ZEB2 Is Required to Maintain the Tissue-Specific Identities of Macrophages. *Immunity*. 2018; 49(2):312–25 e5. <https://doi.org/10.1016/j.immuni.2018.07.004> PMID: 30076102
34. Cain DW, O'Koren EG, Kan MJ, Womble M, Sempowski GD, Hopper K, et al. Identification of a tissue-specific, C/EBPbeta-dependent pathway of differentiation for murine peritoneal macrophages. *J Immunol*. 2013; 191(9):4665–75.
35. Ciofani M, Madar A, Galan C, Sellars M, Mace K, Pauli F, et al. A validated regulatory network for Th17 cell specification. *Cell*. 2012; 151(2):289–303. <https://doi.org/10.1016/j.cell.2012.09.016> PMID: 23021777
36. Edwards SC, Hedley A, Hoevenaer WHM, Glauner T, R W, Kilbey A, et al. Single-cell analysis uncovers 1 differential regulation of lung $\gamma\delta$ T cell subsets by the co-inhibitory molecules, PD-1 and TIM-3. *bioRxiv*. 2021;2021.07.04.451035;.
37. Guilliams M, De Kleer I, Henri S, Post S, Vanhoutte L, De Prijck S, et al. Alveolar macrophages develop from fetal monocytes that differentiate into long-lived cells in the first week of life via GM-CSF. *J Exp Med*. 2013; 210(10):1977–92. <https://doi.org/10.1084/jem.20131199> PMID: 24043763
38. Olson GS, Murray TA, Jahn AN, Mai D, Diercks AH, Gold ES, et al. Type I interferon decreases macrophage energy metabolism during mycobacterial infection. *Cell Rep*. 2021; 35(9):109195. <https://doi.org/10.1016/j.celrep.2021.109195> PMID: 34077724
39. Huang L, Nazarova EV, Tan S, Liu Y, Russell DG. Growth of *Mycobacterium tuberculosis* in vivo segregates with host macrophage metabolism and ontogeny. *J Exp Med*. 2018; 215(4):1135–52. <https://doi.org/10.1084/jem.20172020> PMID: 29500179
40. Griffiths KL, Ahmed M, Das S, Gopal R, Horne W, Connell TD, et al. Targeting dendritic cells to accelerate T-cell activation overcomes a bottleneck in tuberculosis vaccine efficacy. *Nat Commun*. 2016; 7:13894. <https://doi.org/10.1038/ncomms13894> PMID: 28004802
41. Lim PN, Cervantes MM, Pham LK, Rothchild AC. Alveolar macrophages: novel therapeutic targets for respiratory diseases. *Expert Rev Mol Med*. 2021; 23:e18. <https://doi.org/10.1017/erm.2021.21> PMID: 34823627
42. Correa-Macedo W, Fava VM, Orlova M, Cassart P, Olivenstein R, Sanz J, et al. Alveolar macrophages from persons living with HIV show impaired epigenetic response to *Mycobacterium tuberculosis*. *J Clin Invest*. 2021; 131(22). <https://doi.org/10.1172/JCI148013> PMID: 34473646
43. Verma AK, Bansal S, Bauer C, Muralidharan A, Sun K. Influenza Infection Induces Alveolar Macrophage Dysfunction and Thereby Enables Noninvasive *Streptococcus pneumoniae* to Cause Deadly Pneumonia. *J Immunol*. 2020; 205(6):1601–7. <https://doi.org/10.4049/jimmunol.2000094> PMID: 32796026
44. D'Agostino MR, Lai R, Afkhami S, Khera A, Yao Y, Vaseghi-Shanjani M, et al. Airway Macrophages Mediate Mucosal Vaccine-Induced Trained Innate Immunity against *Mycobacterium tuberculosis* in Early Stages of Infection. *J Immunol*. 2020; 205(10):2750–62. <https://doi.org/10.4049/jimmunol.2000532> PMID: 32998983

45. Gu H, Zeng X, Peng L, Xiang C, Zhou Y, Zhang X, et al. Vaccination induces rapid protection against bacterial pneumonia via training alveolar macrophage in mice. *Elife*. 2021; 10. <https://doi.org/10.7554/eLife.69951> PMID: 34544549
46. Peters JM, Irvine EB, Rosenberg JM, Wadsworth MH, Hughes TK, Sutton M, et al. Protective intravenous BCG vaccination induces enhanced immune signaling in the airways. *bioRxiv*. 2023.
47. Khan N, Downey J, Sanz J, Kaufmann E, Blankenhaus B, Pacis A, et al. M. tuberculosis Reprograms Hematopoietic Stem Cells to Limit Myelopoiesis and Impair Trained Immunity. *Cell*. 2020; 183(3):752–70 e22.
48. Grant RA, Morales-Nebreda L, Markov NS, Swaminathan S, Querrey M, Guzman ER, et al. Circuits between infected macrophages and T cells in SARS-CoV-2 pneumonia. *Nature*. 2021; 590(7847):635–41. <https://doi.org/10.1038/s41586-020-03148-w> PMID: 33429418
49. Berry MP, Graham CM, McNab FW, Xu Z, Bloch SA, Oni T, et al. An interferon-inducible neutrophil-driven blood transcriptional signature in human tuberculosis. *Nature*. 2010; 466(7309):973–7. <https://doi.org/10.1038/nature09247> PMID: 20725040
50. Zak DE, Penn-Nicholson A, Scriba TJ, Thompson E, Suliman S, Amon LM, et al. A blood RNA signature for tuberculosis disease risk: a prospective cohort study. *Lancet*. 2016; 387(10035):2312–22. [https://doi.org/10.1016/S0140-6736\(15\)01316-1](https://doi.org/10.1016/S0140-6736(15)01316-1) PMID: 27017310
51. Esaulova E, Das S, Singh DK, Chorenno-Parra JA, Swain A, Arthur L, et al. The immune landscape in tuberculosis reveals populations linked to disease and latency. *Cell Host Microbe*. 2021; 29(2):165–78 e8. <https://doi.org/10.1016/j.chom.2020.11.013> PMID: 33340449
52. Antonelli LR, Gigliotti Rothfuchs A, Goncalves R, Roffe E, Cheever AW, Bafica A, et al. Intranasal Poly-IC treatment exacerbates tuberculosis in mice through the pulmonary recruitment of a pathogen-permissive monocyte/macrophage population. *J Clin Invest*. 2010; 120(5):1674–82. <https://doi.org/10.1172/JCI40817> PMID: 20389020
53. Redford PS, Mayer-Barber KD, McNab FW, Stavropoulos E, Wack A, Sher A, et al. Influenza A virus impairs control of *Mycobacterium tuberculosis* coinfection through a type I interferon receptor-dependent pathway. *J Infect Dis*. 2014; 209(2):270–4. <https://doi.org/10.1093/infdis/jit424> PMID: 23935205
54. Mayer-Barber KD, Andrade BB, Barber DL, Hieny S, Feng CG, Caspar P, et al. Innate and adaptive interferons suppress IL-1alpha and IL-1beta production by distinct pulmonary myeloid subsets during *Mycobacterium tuberculosis* infection. *Immunity*. 2011; 35(6):1023–34.
55. Zhang B, Moorlag SJ, Dominguez-Andres J, Bulut O, Kilic G, Liu Z, et al. Single-cell RNA sequencing reveals induction of distinct trained-immunity programs in human monocytes. *J Clin Invest*. 2022; 132(7). <https://doi.org/10.1172/JCI147719> PMID: 35133977
56. Lipscomb MF, Lyons CR, Nunez G, Ball EJ, Stastny P, Vial W, et al. Human alveolar macrophages: HLA-DR-positive macrophages that are poor stimulators of a primary mixed leukocyte reaction. *J Immunol*. 1986; 136(2):497–504. PMID: 2934472
57. Lyons CR, Ball EJ, Toews GB, Weissler JC, Stastny P, Lipscomb MF. Inability of human alveolar macrophages to stimulate resting T cells correlates with decreased antigen-specific T cell-macrophage binding. *J Immunol*. 1986; 137(4):1173–80. PMID: 2426354
58. Toews GB, Vial WC, Dunn MM, Guzzetta P, Nunez G, Stastny P, et al. The accessory cell function of human alveolar macrophages in specific T cell proliferation. *J Immunol*. 1984; 132(1):181–6. PMID: 6228577
59. Andersen P, Scriba TJ. Moving tuberculosis vaccines from theory to practice. *Nat Rev Immunol*. 2019; 19(9):550–62. <https://doi.org/10.1038/s41577-019-0174-z> PMID: 31114037
60. Srivastava S, Ernst JD. Cutting edge: Direct recognition of infected cells by CD4 T cells is required for control of intracellular *Mycobacterium tuberculosis* in vivo. *J Immunol*. 2013; 191(3):1016–20. <https://doi.org/10.4049/jimmunol.1301236> PMID: 23817429
61. Hilligan KL, Namasivayam S, Clancy CS, O'Mard D, Oland SD, Robertson SJ, et al. Intravenous administration of BCG protects mice against lethal SARS-CoV-2 challenge. *J Exp Med*. 2022; 219(2). <https://doi.org/10.1084/jem.20211862> PMID: 34889942
62. Rothchild AC, Mai D, Aderem A, Diercks AH. Flow Cytometry Analysis and Fluorescence-activated Cell Sorting of Myeloid Cells from Lung and Bronchoalveolar Lavage Samples from *Mycobacterium tuberculosis*-infected Mice. *Bio Protoc*. 2020; 10(10). <https://doi.org/10.21769/bioprotoc.3630> PMID: 32995363
63. Wu TD, Nacu S. Fast and SNP-tolerant detection of complex variants and splicing in short reads. *Bioinformatics*. 2010; 26(7):873–81. <https://doi.org/10.1093/bioinformatics/btq057> PMID: 20147302
64. Robinson MD, McCarthy DJ, Smyth GK. edgeR: a Bioconductor package for differential expression analysis of digital gene expression data. *Bioinformatics*. 2010; 26(1):139–40. <https://doi.org/10.1093/bioinformatics/btp616> PMID: 19910308

65. Liberzon A, Birger C, Thorvaldsdottir H, Ghandi M, Mesirov JP, Tamayo P. The Molecular Signatures Database (MSigDB) hallmark gene set collection. *Cell Syst.* 2015; 1(6):417–25. <https://doi.org/10.1016/j.cels.2015.12.004> PMID: 26771021
66. Subramanian A, Tamayo P, Mootha VK, Mukherjee S, Ebert BL, Gillette MA, et al. Gene set enrichment analysis: a knowledge-based approach for interpreting genome-wide expression profiles. *Proc Natl Acad Sci U S A.* 2005; 102(43):15545–50. <https://doi.org/10.1073/pnas.0506580102> PMID: 16199517
67. Chen J, Cheung F, Shi R, Zhou H, Lu W, Consortium CHI. PBMC fixation and processing for Chromium single-cell RNA sequencing. *J Transl Med.* 2018; 16(1):198. <https://doi.org/10.1186/s12967-018-1578-4> PMID: 30016977
68. Stuart T, Butler A, Hoffman P, Hafemeister C, Papalexi E, Mauck WM 3rd, et al. Comprehensive Integration of Single-Cell Data. *Cell.* 2019; 177(7):1888–902 e21. <https://doi.org/10.1016/j.cell.2019.05.031> PMID: 31178118
69. Heng TS, Painter MW, Immunological Genome Project C. The Immunological Genome Project: networks of gene expression in immune cells. *Nat Immunol.* 2008; 9(10):1091–4. <https://doi.org/10.1038/ni1008-1091> PMID: 18800157
70. Aran D, Looney AP, Liu L, Wu E, Fong V, Hsu A, et al. Reference-based analysis of lung single-cell sequencing reveals a transitional profibrotic macrophage. *Nat Immunol.* 2019; 20(2):163–72. <https://doi.org/10.1038/s41590-018-0276-y> PMID: 30643263
71. Cao J, Spielmann M, Qiu X, Huang X, Ibrahim DM, Hill AJ, et al. The single-cell transcriptional landscape of mammalian organogenesis. *Nature.* 2019; 566(7745):496–502. <https://doi.org/10.1038/s41586-019-0969-x> PMID: 30787437
72. Khan A, Mathelier A. Intervene: a tool for intersection and visualization of multiple gene or genomic region sets. *BMC Bioinformatics.* 2017; 18(1):287. <https://doi.org/10.1186/s12859-017-1708-7> PMID: 28569135